FC MEDIATED PAN-SARBECOVIRUS PROTECTION AFTER ALPHAVIRUS VECTOR VACCINATION

Lily E. Adams[1]; Sarah R. Leist[2]; Kenneth H. Dinnon III[1]; Ande West[2,4]; Kendra L. Gully[2,3]; Elizabeth J. Anderson[3]; Jennifer F. Loome[1]; Emily A. Madden[1]; John M. Powers[2]; Alexandra Schäfer[2]; Sanjay Sarkar[4]; Izabella N. Castillo[1], Jenny S. Maron[7]; Ryan P. McNamara[7]; Harry L. Bertera[7]; Mark R. Zweigert[2]; Jaclyn S. Higgins[1]; Brea K. Hampton[4]; Lakshmanane Premkumar[1]; Galit Alter[7]; Stephanie A. Montgomery[5,8]; Victoria K. Baxter[3,5+]; Mark T. Heise[1,4,6+*]; and Ralph S. Baric[1,2,6+*]

[1]Department of Microbiology & Immunology, [2]Department of Epidemiology, [3]Division of Comparative Medicine, [4]Department of Genetics, [5]Department of Pathology and Laboratory Medicine, [6]Rapidly Emerging Antiviral Drug Discovery Initiative, University of North Carolina at Chapel Hill, Chapel Hill, NC, USA.

[7]Ragon Institute of MGH, MIT, and Harvard University, Cambridge, MA, USA

[8]Dallas Tissue Research, Dallas, TX, USA

[+]Senior author. [*]Corresponding author.

ABSTRACT

Two group 2B β-coronaviruses (sarbecoviruses) have caused regional and global epidemics in modern history. The mechanisms of cross protection driven by the sarbecovirus spike, a dominant immunogen, are less clear yet critically important for pan-sarbecovirus vaccine development. We evaluated the mechanisms of cross-sarbecovirus protective immunity using a panel of alphavirus-vectored vaccines covering bat to human strains. While vaccination did not prevent virus replication, it protected against lethal heterologous disease outcomes in both SARS-CoV-2 and clade 2 bat sarbecovirus HKU3-SRBD challenge models. The spike vaccines tested primarily elicited a highly S1-specific homologous neutralizing antibody response with no detectable cross-virus neutralization. We found non-neutralizing antibody functions that mediated cross protection in wild-type mice were mechanistically linked to FcgR4 and spike S2-binding antibodies. Protection was lost in FcR knockout mice, further supporting a model for non-neutralizing, protective antibodies. These data highlight the importance of FcR-mediated cross-protective immune responses in universal pan-sarbecovirus vaccine designs.

INTRODUCTION

Three β-coronaviruses (βCoVs) have caused epidemic and pandemic disease in human populations in the 21st century. The 2002-2004 severe acute respiratory coronavirus (SARS-CoV) and the 2019 SARS-CoV-2 (the causative agent of the COVID-19 pandemic) viruses represent prototype clade 1a and clade 1b group 2B βCoVs, which belong to the subgenus sarbecoviruses. SARS-CoV and SARS-CoV-2 likely emerged from bat reservoirs either through intermediate host transmission events or through direct spread into human populations (1, 2). The subgenus sarbecovirus includes other highly heterogeneous epidemic, pandemic, and zoonotic strains poised for emergence and cross-species transmission to novel mammalian hosts. Other sarbecoviruses identified in bat or mammalian reservoirs, including SHC014 and WIV1, can use human ACE2 receptors for entry and replicate efficiently in primary human cells (3–11). Due to global efforts, safe and effective vaccines against SARS-CoV-2 are approved for use (12–14) and next-generation vaccines including those vectored by alphaviruses are under development (15–17). The accelerated approval of SARS-CoV-2 vaccines is the result of decades of basic and applied research (12). However, current SARS-CoV-2 spike-based vaccines provide limited protection against heterologous bat sarbecoviruses, as well as recently emerged SARS-CoV-2 variants of concern (VOC) (18). The extent and complex immunologic mechanisms regulating cross protection against closely related and distant strains remains poorly understood but is critical for pan-coronavirus vaccine design, human health, and public health preparedness.

The sarbecovirus spike glycoprotein is a class I viral fusion protein roughly 1,300 amino acids in length that trimerizes upon folding. Spike is divided into an amino-terminal S1 subunit, containing the receptor-binding domain, and a carboxy-terminal S2 subunit, driving membrane fusion. The S1 subunit is further subdivided into a highly variable N-terminal domain (NTD) and a receptor binding domain (RBD), which engages the ACE2 receptor. Subtle molecular communication networks across domains are thought to influence epitope presentation, as evidenced by druggable targets in the NTD that interrupt distal RBD interactions with ACE2 as well as the identification of spike mutations outside of the RBD that stabilize receptor interaction (19, 20). As such, structural features of the spike are likely to impact vaccine cross-protection. Recent work has characterized the immune response against distinct Sarbecovirus spike proteins following homologous or heterologous vaccination (21–24). Cross-reactive T cells and antibodies recognize broadly conserved epitopes across SARS-CoV-2, other sarbecoviruses, and endemic (common-cold) β-coronaviruses. However, the role of these epitopes in protective immunity remains a subject of rigorous investigation (22, 25, 26). After SARS-CoV-2 natural infection or vaccination, the spike RBD, NTD, and S2 domains stimulate neutralizing and non-

neutralizing antibody responses. Among sarbecoviruses, potent, broadly protective, neutralizing antibodies primarily target specific epitopes in the RBD and S2 portions of the spike glycoprotein (23, 27–32), typically targeting epitope bins RBD-6 and RBD-7 (33, 34). However, neutralizing antibody activity and function have not been correlated, as it is sometimes difficult to predict whether potent cross-reactive neutralizing antibodies that target spike will sufficiently protect *in vivo* (34). Although less widely studied, several studies have shown that antibody FcR-mediated effector functions are critical in protective immunity (35–39). Fc receptors have high affinity for IgG subtypes and are cell surface receptors on monocytes, macrophages, and neutrophils; FcR recognition of the antibody Fc region stimulates effector cell function like NK cell-mediated lysis, neutrophil degranulation, and ADCP (40). Thus, FcR effector function may be a key correlate for next generation vaccine development and improvement.

Here, we utilized a Venezuelan equine encephalitis virus 3526 replicon particle (VRP3526) (41) as a platform to evaluate mechanisms of cross protection after pandemic and pre-emergent coronavirus spike glycoprotein vaccination in mice, followed by lethal SARS-CoV-2 challenge (42). VRP vectors induce robust cellular and humoral immune responses after vaccination and VRP spike vaccines protect against SARS-CoV and SARS-CoV-2 *in vivo* (43, 44). In the present study, contemporary human coronavirus spikes elicited no protection against weight loss, mortality, or virus replication after SARS-CoV-2 challenge. While VRP delivered homologous SARS-CoV-2 spike vaccines protected against weight loss, lethal disease, and virus replication after homologous challenge, heterologous VRP sarbecovirus spike vaccines conferred cross protection against weight loss and death, but provided limited reductions in SARS-CoV-2 MA10 replication in young and aged animals. While homologous protection correlated with potent neutralizing antibody responses that principally targeted the S1 subdomains, no cross-neutralizing antibodies were detected against the heterologous sarbecovirus strains. Rather, systems serology (45), *in vitro* studies, and passive antibody transfer experiments in wild-type and Fc-receptor deficient mice implicated an FcR-driven mechanism targeting S2, such as antibody-dependent cellular phagocytosis (ADCP). These results build support for universal sarbecovirus vaccine designs that include FcR-mediated cross protection, coupled with potent cross-neutralizing antibody responses.

RESULTS

Venezuelan equine encephalitis virus replicon particle assembly produced high titer vaccines to potently express coronavirus spike proteins *in vivo*

Venezuelan equine encephalitis virus 3526 replicon particles (VRPs) are BSL2, non-select, replication-deficient vectors derived from a live attenuated strain (41). They are assembled using a tripartite RNA-based assembly scheme (**Fig. 1A**), thus generating a self-amplifying, single cell hit RNA vaccine platform. We generated replicon particles (VRPs) expressing spike proteins from several α- and β-CoVs that included three common-cold CoVs, OC43, NL63, and HKU1 (**Fig. 1B, green**), as well as pandemic (SARS-CoV, SARS-CoV-2) and pre-emergent sarbecoviruses circulating in animal reservoirs (RaTG13, HKU3, WIV1, SHC014) (**Fig. 1B, red**). The sarbecovirus spike proteins were separated into three groups based on amino acid similarity: clade 1a (SARS-CoV, SHC014, WIV1), 2 (HKU3), and 1b (SARS-CoV-2, RaTG13) (**Fig. 1A**) (46). The clade 1b virus RaTG13 spike protein is 97.4% identical to the SARS-CoV-2 spike protein, the clade 2 virus HKU3 spike protein shares 75.8% identity to the SARS-CoV-2 spike protein, and the clade 1a virus spike proteins share 75.6-78.6% identity to the SARS-CoV-2 spike protein. Clade 2 HKU3 spike protein shares 78.1-78.8% identity to the clade 1a spike proteins (**Table 1**). All VRP preparations achieved particle titers exceeding $2x10^6$ IU/mL, sufficient for vaccination in a mouse model (**Fig. 1C)** (41). Immunofluorescent staining for the highly conserved spike S2 domain verified spike expression in mammalian cells infected by VRPs (**Fig. 1D**).

VRP-vectored sarbecovirus spike proteins protect against severe SARS-CoV-2 disease in young mice

To test the VRP 3526 platform and evaluate the capacity for spike protein elicited cross-protection, we utilized a lethal mouse model for SARS-CoV-2 disease. Groups (n = 8-10) of 8-10 week aged female BALB/cAnNHsd (BALB/c) mice were vaccinated with a low dose of $2x10^4$ IU VRP encoding each of the different spike vaccines by footpad injection then boosted on day 21 with the homologous spike VRP. At 21 days post-boost, (now 14-16 week aged) BALB/c mice were challenged with 10^4 PFU SARS-CoV-2 MA10 (42) intranasally. Virus titer after challenge is a sensitive measure of vaccine performance, and reductions in titer are often correlative to vaccine efficacy (12, 47). However, only the VRP SARS-CoV-2 spike vaccine elicited nearly complete protection from homologous virus replication. In contrast, the clade 1b VRP RaTG13 spike vaccination resulted in slight, but significant reductions in virus titers on day 2 (1 log reduction, 10-fold) and 5 (3 log reduction, 1,000-fold) post infection, as compared to the GFP vaccinated controls. In animals vaccinated with clade 2 VRP HKU3 spike, SARS-CoV-2 MA10 titers were significantly reduced by about 1.5 and 3 logs (~30- and 1,000-fold) on days 2 and 5 post infection, compared to GFP control vaccinated animals. We also saw slight, but

significant, reductions in virus titers in mice vaccinated with highly heterogeneous clade 1a strains (SARS-CoV, WIV1 and SHC014) on day 2. However, titers were reduced by about 2 logs on day 5 post infection (**Fig. 2A**).

Consistent with VRP vaccine effects on viral replication, we observed a range of protection outcomes following virus challenge. Bronchoconstriction and airway resistance in the lungs of challenged mice are a representative disease metric measured by whole-body plethysmography that mirrors disease in humans (48). Using this method, we tracked respiratory function through the duration of the experiment and analyzed the overall difference in lung function between vaccine groups via area under the curve calculations. Overall, we found that clade 1b and clade 2 vaccines effectively protected against bronchoconstriction (Rpef) and airway resistance (PenH) after SARS-CoV-2 MA10 challenge **(Fig. 2B**), accordant with reduced clinical disease. In contrast, clade 1a vaccinated animals had significantly increased respiratory dysfunction and clinical disease when compared to uninfected controls, indicating reduced protection. As additional measures of disease severity, we monitored weight loss and assessed lung pathology by scoring gross discoloration (GLD), diffuse alveolar damage (DAD), and acute lung injury (ALI) following SARS-CoV-2 challenge. Homologous SARS-CoV-2 challenge in VRP SARS-CoV-2 spike vaccinated animals resulted in minimal weight loss (**Fig. 2C**) and GLD (**Fig. 2F**), and as such animals were fully protected against significant SARS-CoV-2 disease. In contrast, the other zoonotic and pandemic CoV spike proteins partially protected from clinical disease compared to controls. For example, the clade 1b CoV spike proteins protected against severe SARS-CoV-2 disease, resulting in little (~10%-RaTG13) to no measurable weight loss (SARS-CoV-2) and minimal GLD at the time of tissue harvest (**Fig. 2C, F**). Under identical conditions, clade 1a spike (SARS-CoV, WIV1 and SHC014) vaccines elicited low level intermediate protection after SARS-CoV-2 MA10 challenge, resulting in more weight loss, ranging between 10-15% body weight lost, and notable increases in GLD (**Fig. 2E, F**). Despite being as distant as the clade 1a CoV spikes were from the SARS-CoV-2 spike (Table 1), the clade 2 HKU3 spike vaccine elicited near full protection against disease with ~5% weight loss and minimal lung discoloration at tissue harvest (**Fig. 2D, F**). In addition to antigenic distance, the HKU3 spike protein also contains deletions in both the NTD and RBD when compared to the SARS-CoV-2 spike protein (**Fig. S1**). Thus, the protection elicited by VRP HKU3 spike after SARS-CoV-2 heterologous challenge is particularly noteworthy. Within vaccine groups where mice were partially protected from disease, such as WIV1 spike vaccine, disease outcomes ranged from mild disease (mild weight loss and lung discoloration) to severe disease (significant weight loss and severe lung discoloration), suggesting that this protective mechanism is subject to

strain-specific variation, resulting in highly variable disease outcomes. Overall, we calculated a robust negative correlation coefficient (-0.76) between disease metrics of GLD and area under the curve of percent body weight as well as a strong positive correlation (0.72) between virus titers day 2 and day 5 post infection. The slight, but incomplete, reduction in virus titer suggests that protection was likely not mediated by the presence of potent cross-neutralizing antibodies with the ability to prevent infection. However, we calculated a negative correlation coefficient (-0.68) between viral titer two days post infection and disease severity as measure by area under the curve of percent body weight through the duration of the study, indicating virus titer may still be predictive of disease severity in our model.

Consistent with prior established work (42), histological examination (**Fig. 2G, H**) of lung sections stained for hematoxylin and eosin at 5 days post infection identified regions of severe disease in mock vaccinated, infected animals, including infiltration of neutrophils in the interstitial and alveolar spaces, alveolar septal thickening, cell sloughing and proteinaceous debris in the airspaces, and hyaline membrane formation (**Fig. 2I**). Using previously described scoring metrics for diffuse alveolar damage (DAD) and acute lung injury (ALI), histologic sections revealed large numbers of infiltrating immune cells, increased membrane thickness, and proteinaceous debris in the airspaces (42) (**Fig. 2I, red, blue, black**). Consistent with other metrics reported in this study (e.g. weight loss), mice vaccinated with the homologous spike demonstrated protection from SARS-2-induced lung pathology, with baseline-equivalent DAD and ALI scores (41) (**Fig. 2G, H, I**). Heterologous vaccines that were associated with greater GLD scores and thus only partial protection (e.g. WIV1) demonstrated more severe tissue damage and higher DAD and ALI scores. Vaccines that were more protective (e.g. HKU3) resulted in lower DAD and ALI scores comparable to the SARS-2 vaccinated group.

We also used our SARS-CoV-2 mouse lethal challenge model to evaluate whether vaccination with VRPs expressing spikes of contemporary common cold human β-CoV, which share conserved S2 epitopes with epidemic and pre-emergent β-CoV (49, 50) would protect against SARS-CoV-2 disease. We found that single exposures (single component, two doses) of contemporary human coronavirus spike proteins did not protect against severe SARS-CoV-2 disease and mortality in young mice (**Fig. S2 A, C**), nor did these vaccines reduce viral replication efficiency (**Fig. S2 B**). In contrast to the Group 2B coronavirus vaccinated mice, a large percentage (>50% in most cases) of common cold spike vaccinated mice died when compared to those vaccinated with VRP SARS-CoV-2 spike (**Fig. S2 C**).

Evaluating the potential for aberrant immunity after vaccination is especially important as killed/inactivated CoV vaccines have been reported to induce a pro-inflammatory and Th2 skewed immune response, commonly associated with immune pathology (47, 51). Using a BioPlex Cytokine Immunoassay, we measured the cytokine responses after challenge in vaccinated mice on days 2 and 5 post infection. In groups that received heterologous VRP spike vaccines, we did not detect elevated Th2 cell cytokine signatures (IL-4, IL-5, IL-13), rather VRP vaccines elicited a strong Th1 signature (IL-12, TNF-α, IFN-γ) which is commonly associated with a protective immune response (41). Additionally, in contrast to the groups vaccinated with the homologous SARS-CoV-2 spike, groups vaccinated with the heterologous sarbecovirus VRP spikes demonstrated elevated pro-inflammatory cytokine responses in the lung two days post-SARS-CoV-2 MA10 challenge (IL-1β, IFN-γ, TNF-α, IL-6) (**Fig. S3**). Altogether, this suggests the VRP sarbecovirus spike vaccines elicited a protective immune response against SARS-CoV-2 infection.

VRP-vectored sarbecovirus spike proteins protect against severe SARS-CoV-2 disease in old mice

To test the efficacy of the VRP platform and evaluate the potential for cross-protection in an aging population, we utilized the SARS-CoV-2 MA10 lethal challenge model in aged (1-year old) mice. Mice were immunized with $2x10^4$ IU VRP by footpad inoculation following a prime/boost schedule on days 0 and 21. Three weeks post boost, mice were challenged with 10^3 PFU (~1 LD_{50}, typically 50% mortality) SARS-CoV-2 MA10 intranasally (**Fig. 3A-F**). We observed near complete protection in our homologous vaccinated, aged mouse model, as animals challenged with SARS-CoV-2 MA10 experienced ~5% weight loss before recovery (**Fig. 3A**). Importantly, VRP SARS-CoV-2 spike vaccinated animals were also significantly protected from GLD upon tissue harvest on days 2 and 5 post infection (**Fig. 3D**). Moreover, virus titers were reduced by 5 and 3 logs on day 2 and 5 post infection, a significant reduction when compared to controls (**Fig. 3E**). In contrast, clade 1b VRP RaTG13 spike vaccinated animals showed some protection from clinical disease as measured by limited weight loss (~8%) and GLD on days 2 and 5 post infection, as compared to mock vaccinated controls (**Fig. 3A, D**). Clade 2 VRP HKU3 spike vaccinated animals also showed limited weight loss (~10%), GLD, and slight reduction in virus titer on days 2 and 5 post infection, which were significantly different from controls. Clade 1a VRP spike vaccines elicited significant but variable levels of protection in the aged mouse model after SARS-CoV-2 MA10 challenge (**Fig. 3B, D**). Based on protection from weight loss and lung discoloration scores, clade 1a VRP vaccines were protective when compared to mock

vaccinated controls on days 2 and 5 post infection (**Fig. 3C, D**). However, clade 1a vaccines did not protect against virus replication on day 2, as modest but not significant ~1 log reductions were noted in VRP WIV1 and VRP SHC014 vaccinated animals on day 5. Reductions in respiratory function generally correlated with overall disease severity, as measured by weight loss and GLD (**Fig. 3F**). Compared to young mice, SARS-CoV-2 replicated to higher titers in the lungs of the old mice with more breakthrough replication in the homologous vaccinated mice (**Fig. 3E**).

As aged animals are significantly more vulnerable to higher SARS-CoV-2 MA10 challenge doses (42), we next determined if the VRP sarbecovirus spike vaccine panel could protect against a 10-fold higher, 10^4 challenge dose, which typically results in 85% mortality. Mice vaccinated with VRP SARS-CoV-2 spike were fully protected from severe disease and mortality through day 5 post infection. In contrast, mice vaccinated with other clade 1a, 1b, or clade 2 heterologous VRP spike vaccines experienced equivalent weight loss as mock vaccinated controls (**Fig. S4**) and mortality rates of 25-75% (**Fig. 3G**), indicating the cross-protection elicited in our model has dramatic potential to vary in an aging population, especially as a function of infectious dose.

VRP SARS-CoV-2 spike protects against disease in heterologous sarbecovirus infection

The clade 2 HKU3 strain cannot infect primate cells and does not use an ortholog human, civet, select bat, or mouse ACE2 receptor for docking and entry (11). However, more recent studies suggest that some clade 2 strains can utilize bat ACE2 molecules for entry if isolated from their natural bat host species (52), which suggests clade 2 sarbecoviruses may become an emergent threat in the future. Although the HKU3 spike is phylogenetically distant from clade 1 strains (**Table 1**), vaccination elicited a good protective profile against SARS-CoV-2 MA10 (**Fig. 2**). As HKU3 could emerge by mutation or RNA recombination, we next evaluated whether the VRP SARS-CoV-2 spike vaccine would protect against clade 2 heterologous challenge. 8-10 week old mice were vaccinated and boosted with VRP HKU3, VRP SARS-CoV-2, and VRP GFP vaccines as previously described. Vaccinated mice were then infected intranasally with the mouse-adapted clade 2 bat sarbecovirus designated HKU3-SRBD MA, a virus that can infect mammalian cells and cause disease in mice (11, 53). The homologous HKU3 vaccinated animals were fully protected from weight loss, GLD, and showed a significant 4-log reduction in titer after HKU3-SRBD challenge (**Fig. 4A-C**). In contrast, the heterologous VRP SARS-CoV-2 vaccine attenuated HKU3-SRBD disease severity as evidenced by ~15% body weight loss (**Fig. 4A**), a recovery of body weight after 3 days, and modest reductions in GLD scores when

compared to mock vaccinated animals (**Fig. 4B**). Modest but significant ~5- and 10-fold reductions in virus titer were also noted on days 2 and 5 post infection, respectively, in VRP SARS-CoV-2 vaccinated mice when compared to VRP GFP vaccinated control (**Fig. 4C**). As such, we observed a cross-protective phenotype mediated by VRP spike vaccines in two unique challenge models, prompting further mechanistic investigation.

VRP spike vaccinations induce non-neutralizing, cross-reactive antibodies

Each VRP spike vaccine elicited a potent serologic IgG response against the SARS-CoV-2 spike protein (**Fig. 5A, left**). Total IgG titers ranged from 1×10^4 to 5×10^4. The VRP spike vaccines also elicited a potent IgG response against the SARS-CoV-2 receptor binding domain (RBD**, Fig. 5A, middle**), though at about a two-fold reduction in potency. Additionally, mice vaccinated with VRP RaTG13 did not produce significant IgG against the SARS-CoV-2 RBD, despite inducing notable IgG against the SARS-CoV-2 N-terminal domain, comparable to the homologous VRP SARS-CoV-2 vaccine (NTD, **Fig. 5A, right**). The NTD is fairly well conserved between SARS-CoV-2 and RaTG13 (98.3% amino acid identity), while the RBD is more diverged (89.3%, more divergence in the receptor-binding motif), so these results were not unexpected. After VRP vaccination (**Fig. 5B**), we detected a strong IgG2a skew in antibody titers in VRP spike antigen-vaccinated mice, but not in GFP control vaccinated mice, indicating that vaccination with the sarbecovirus spikes induced a protective Th1 response (54). We also observed a marked vaccine antigen specific grouping in the ratio of IgG2a to IgG1; for example, the VRP SARS-CoV-2 vaccine (blue) elicited a more IgG2a skewed antibody response against the SARS-CoV-2 spike protein than the VRP RaTG13 vaccine (red). Further analyses demonstrated high reactivity towards full-length spike with little-to-no preference for IgG2a recognition of S1 or S2 (**Fig. 5C**). Given the presence of cross-reactive antibody responses elicited by VRP-spike vaccines, we then tested the neutralizing antibody response in a series of live-virus assays. Overall, we detected neutralizing antibodies only in the homologous VRP SARS-CoV-2 vaccine group with an IC_{50} of ~1:700 but did not detect any cross-neutralizing antibody responses between any of the other VRP vaccine groups and luciferase reporter SARS-CoV-2, except for some low-level SARS-CoV-2 neutralizing titers in a subset of VRP RaTG13 vaccinated animals (**Fig. 5D**). Additionally, VRP SHC014 sera neutralized reporter virus SHC014 with an IC_{50} of ~1:800 (**Fig. 5F**), but there was also no detectable neutralization of the SHC014 virus by VRP SARS-CoV-2 sera.

Using a luciferase reporter system to detect spike NTD, RBD and S1 domain-specific neutralizing antibodies (18, 34), we determined that the majority of VRP SARS-CoV-2 spike

neutralizing antibodies targeted the RBD (amino acids 332-528) and the C-terminal segment of S1 (RBD+, amino acids 332-685). Additionally, despite clear evidence of at least 4 neutralizing epitopes in the N-terminal domain (NTD, amino acids 13-305) (33), the VRP SARS-CoV-2 spike vaccines failed to elicit measurable neutralizing antibody titers against the SARS-CoV-2 NTD or S2 domain (**Fig. 5E**). We also mapped the domain specific neutralizing antibody responses elicited by animals vaccinated with the VRP SHC014 spike. In this loss of function assay, VRP SHC014 spike elicited neutralizing antibodies preferentially targeted the NTD and RBD+ regions. The complete loss of neutralization was noted when larger segments of the spike protein were exchanged in the reporter system – either RBD+ or the region spanning from the beginning of the NTD to the end of the RBD (NTD-RBD, amino acids 13-528). This also indicates that SHC014 homologous neutralizing antibodies preferentially target highly specific epitopes in the SHC014 spike S1 region (**Fig. 5G**). Our data suggests that neutralizing antibody responses elicited by VRP spike vaccines are highly type-and domain-specific, supporting the hypothesis that cross-neutralizing antibodies do not drive VRP cross-protection between sarbecoviruses.

Given the inconsistency between neutralizing antibodies and cross protection, we further employed systems serology to characterize the overall humoral architecture in response to our VRP candidates (37, 45) (**Fig. S5**). An initial multivariate analysis (partial least squares discriminant analysis, or PLS-DA) demonstrated a strong clustering of challenged animals away from baseline for both Fab (**Fig. 5H**) and FcR (**Fig. 5J**) binding antibodies. Individual features that separated groupings were identified. Interestingly, Fc-mediated, non-neutralizing functions such as antibody dependent complement deposition (ADCD) and antibody-dependent cellular phagocytosis (ADCP) were among the highest ranked. We validated this through clustering these functional assays with both Fab and FcR binding profiles (**Fig. 5I**, **K**). Similar to our previous analysis, PLS-DA identified that humoral recognition of both S1 and S2 subregions was driving the phenotype, and not simply RBD-responsive antibodies, which bear the majority of neutralizing activity.

To more closely delineate protective signatures stimulated by the VRP spike vaccines, we performed cross-correlative analyses for the entire data set as well as each VRP spike vaccine (**Fig. S6**). To summarize the correlation matrices and identify trends, we highlighted associations with strong, significant correlations ($0.7 – 1$, $p < 0.05$) from each VRP spike vaccine, focusing on IgG2a, functional assays, and Fc-gamma receptors FcgR3/R4 stimulated by the SARS-CoV-2 spike antigens (**Fig. 6A**). Strikingly, while numerous S1 and S2 correlates

were identified, there was little overlap between the two. Recognition of S2 by various VRP spike sera was tied to Fc-effector mediated functions, while S1 demonstrated strong correlations with FcgR4, but was not statistically tied to effector functions (**Fig. 6A**, **B**). Using a peptide scanning array that spanned the majority of S2, we identified that heptad repeat region 2 (HR2), the fusion peptides (FP), and the stalk subregions drove much of the IgG2a recognition. Notably, we found that full spike, S2, and S2 subdomain-specific IgG2a and the phagocytic functional assays (ADNP/ADCP) had a strong correlation for the more distant heterologous VRP spike vaccines (HKU3, SARS-CoV, WIV1, SHC014). We also found that the VRP SARS-CoV-2 and the more protective spike vaccines (HKU3, RaTG13) IgG2a correlated with ADCD (**Fig. 6A**). Generally, FcR stimulation was clade-dependent and in some cases similar to the clade-dependent *in vivo* protection characterized above. FcgR4 was most activated by clade 1b and 2 VRP spike sera (SARS-CoV-2, RaTG13, and HKU3), and less so by clade 1a VRP spike sera (SARS, SHC014, and WIV1) (**Fig. 6B**). Consequently, we evaluated the capacity for the VRP spike serum to stimulate antibody-dependent cellular phagocytosis (ADCP) and neutrophil phagocytosis (ADNP) against the SARS-CoV-2 full spike as previously described at the univariate level (37, 55). Overall, we found notable and significant increases in ADNP (**Fig. 6C**) as well as significant ADCP against the SARS-CoV-2 full spike (**Fig. 6D**) in VRP spike vaccine sera. However, the magnitude of response was not clearly clade-dependent.

Though we identified variable responses, our data as compiled by systems serology analysis demonstrate that VRP spike-specific, non-neutralizing antibodies stimulate FcR effector functions. These functions are mechanistically linked to FcgR4 binding IgG2a, and additional heatmap analysis of the heterologous VRP spike sera (**Fig. S7**) indicated that, not only did IgG2a cluster very well with itself, but the heptad repeat regions (HR1, HR2), and stalk subdomains of spike also exhibited the greatest strength of binding (**Fig. S7A**). When evaluating subclass binding within S2, a peptide scanning array also indicated that IgG2a bound with high significance to the HR1, HR2, fusion peptide (FP), and stalk subdomains of S2 (**Fig. S7B**).

Since HKU3 and RaTG13 spike vaccines showed the highest level of protection against heterologous SARS-CoV-2 challenge, we asked whether there was a correlation between domain specific antibody binding and disease severity. The magnitude of VRP HKU3 spike serum IgG2a binding the HR1 shared a very significant correlation (Pearson's $r = 0.92$, $p < 0.05$, $n = 4$) with protection from disease as measured by AUC of body weight maintenance curves. Likewise, VRP RaTG13 sera S2 binding also showed a very significant correlation (Pearson's r

= 0.91, $p < 0.05$, n = 4) with protection from disease. Surprisingly, we found significant correlations between protection from disease and antibody binding in most S2 subdomains for WIV1 but in contrast to most other vaccine groups, failed to detect correlations between protection and functional assays like ADCD and ADCP for WIV1. Under further evaluation, we found that *in vivo* protection elicited by other VRP spike vaccines were linked to S2, but not single domains. Notably the SHC014 VRP spike vaccine was also closely linked to the NTD **(Fig. S7C**). These data suggest that the sum of smaller fractions of cross-reactive antibody responses may also contribute to protection in the context of the more distant, less protective vaccine strains in addition to the capacity of the binding antibodies to stimulate protective FcR effector responses.

These data implicate sequence conservation in linear epitopes of S2, especially HR1, in addition to cellular functional stimulation as a driver of the cross-protective, non-neutralizing antibody response elicited by VRP-vectored sarbecovirus spikes. Within S2, the HR2 subdomain is 100% conserved between the sarbecovirus spikes tested, while the HR1 subdomain contains sequence variation. The HR1 subdomain of RaTG13 and HKU3 is 100% and 98.7% identical to the SARS-CoV-2 HR1 subdomain, respectively. In contrast, the HR1 subdomains of the clade 1a sarbecovirus spikes which showed less protection, share 88.3-89.6% identity to the SARS-CoV-2 spike HR1 (**Fig. S7D**). These results support the hypothesis that the binding of non-neutralizing antibodies to conserved sequences within the HR1 domain may contribute to heterologous protection against SARS-CoV-2 challenge in our model.

VRP spike vaccinations induce antibody-mediated protection via Fc effector mechanism

Given indications of non-neutralizing, antibody-dependent cellular function by serological assays, we conducted a prophylactic passive transfer experiment to further evaluate the role of antiserum in cross protection from clinical disease. Serum from VRP spike (SARS-CoV-2, SARS-CoV, HKU3, and GFP) vaccinated mice was pooled for a given group and then administered intraperitoneally into naïve mice (Taconic and Envigo, Envigo n = 5 reported). Twenty-four hours later, the mice were challenged with 10^4 PFU of SARS-CoV-2 MA10 in a lethal challenge. Importantly, compared to GFP control, SARS-CoV-2 and HKU3 VRP serum recipients experienced significant reductions in weight loss (statistically significant by day 5 post infection), while the SARS-CoV VRP serum recipients developed more severe weight loss that was not significantly reduced compared to control serum recipients (**Fig. 6E**). We also observed significant reductions in GLD scoring by all groups, demonstrating that passive transfer of antibodies mitigated severe/lethal disease (**Fig. 6F**). This was in contrast with detected viral

loads which were exclusively mitigated by VRP SARS-CoV-2 antigen (**Fig. 6G**). This provides further support to the hypothesis that neutralizing antibodies play a substantial role in limiting viral replication and disease, whereas non-neutralizing antibodies primarily mitigate disease pathology. Collectively, these data suggest that there is a clear role for antibodies, albeit non-neutralizing, in vaccine cross protection against SARS-CoV-2.

To further probe the mechanism of VRP spike cross-protection, we vaccinated FcR-deficient BALB/c mice (Taconic, n = 6) before lethal challenge with SARS-CoV-2 MA10. We found that, when Fc effector function is effectively eliminated, protection against SARS-CoV-2 disease in mice afforded by vaccination with VRP HKU3 spike was eliminated (**Fig. 6H-J**). Both rapid/sustained weight loss (**Fig 6H**) and GLD (**Fig. 6I**) were evident in the FcR KO mice immunized with VRP HKU3, and unlike WT mice, were statistically indistinguishable from GFP-vaccinated mice. However, FcR-deficient mice vaccinated with VRP SARS-CoV-2 spike were still protected from clinical disease and virus replication, again consistent with a strong homologous neutralizing antibody response (**Fig. 6J**). This indicates that cross protection is mechanistically linked to FcR-mediated responses despite a potent homologous protective profile.

To further evaluate the role for FcR effector function (e.g. macrophages, neutrophils) in VRP spike cross-protection *in vivo*, we conducted a prophylactic passive transfer experiment in FcR-deficient BALB/c mice (Taconic, n = 5), prior to lethal challenge with SARS-CoV-2 MA10. As evidenced by weight loss (**Fig. 6K**) and GLD scores (**Fig. 6L**), we found that the SARS-CoV-2 spike homologous sera still protected against severe disease in the absence of FcR effector function. Additionally, we found significant reductions in virus titer in the lungs of animals that received VRP SARS-CoV-2 spike sera, again supporting a strong homologous neutralizing antibody response (**Fig. 6M**). However, we found that the heterologous SARS-CoV and HKU3 VRP sera failed to protect in FcR-deficient mice (**Fig. 6L-N**). When compared to wild-type mice as previously described, FcR-deficient mice had increased GLD and increased weight loss, with no decrease in virus titer in the lungs. FcR-deficient mice that received heterologous VRP sera surpassed 20% weight loss on day 5 post infection, indicative of lethal disease. This indicates that strain-specific antibodies capable of neutralization can protect from disease, but cross protection is mechanistically linked to non-neutralizing, FcR-mediated responses.

Altogether, our data indicate that neutralizing antibodies can protect from disease, but are oftentimes limited to homologous challenges after VRP vaccination. Rather, non-neutralizing

FcR function is a primary driver of VRP spike antibody-mediated cross protection from sarbecovirus disease.

DISCUSSION

The emergence of SARS-CoV-2 underscores the tragic global consequences of a recently emerged zoonotic virus. The COVID-19 pandemic has resulted in massive human suffering and global economic upheavals with millions of deaths. When considering the continued spread of SARS-CoV-2 VOC, coupled with large numbers of zoonotic reservoir strains poised for cross species movement, robust countermeasures that elicit broad, cross-protective immune responses offer considerable hope for controlling sarbecovirus epidemics. Though a potent neutralizing antibody response is a benchmark for COVID-19 vaccine efficacy, recent work has identified that SARS-CoV-2 S2P mRNA vaccines elicited limited cross neutralizing antibody titers against heterologous sarbecoviruses and the SARS-CoV-2 Omicron VOC (18, 56, 57). Moreover, several studies have suggested a potential role for non-neutralizing antibody function in protection against SARS-CoV-2 disease (35, 36, 58), highlighting a critical need for identification of additional correlates associated with pan-sarbecovirus protection. As alphavirus replicons are under development as COVID-19 vaccines that induce mucosal, humoral and cellular immune responses, they provide innovative models for understanding cross immune mechanisms (15–17). In the present study, we found that non-neutralizing antibodies can contribute to broad cross-vaccine protective immunity across clade 1a, 1b, and clade 2 sarbecoviruses, with as little as 75% amino acid identity between spike protein amino acid sequences. Our studies further support an important protective role for non-neutralizing antibodies, especially in cases of heterologous virus infection across distant sarbecoviruses, via antibody interactions with FcR effector functions as a driver of protective immunity (36). In addition to T cell immunity (59), a good universal vaccine will likely stimulate multiple arms of the B cell-driven immune response – including potent type-specific, as well as broadly cross-neutralizing and non-neutralizing antibodies that promote FcR effector functions.

Consonant with a potent neutralizing antibody response described previously (44), VRP SARS-CoV-2 spike vaccination prevented severe disease in young mice and significantly reduced virus replication in the airway after SARS-CoV-2 MA10 challenge. Highly potent mRNA vaccines target neutralizing antibody responses to the S1 RBD domain (60, 61) and potent neutralizing antibodies targeting one or more epitopes in the RBD (28), NTD (62), or S2 (63, 64) have been identified in the spike protein. Consonant with established work, we found the homologous neutralizing antibody response stimulated by the VRP platform preferentially targeted the

receptor-binding domain (targeted by VRP SARS-CoV-2 S) and/or the N-terminal domain (both targeted by VRP SHC014 S). S1 is highly divergent across sarbecoviruses, but contains conserved regions that stimulate cross-neutralizing antibodies (28, 34). However, we failed to detect protective levels of cross-neutralizing antibodies elicited by heterologous VRP spike vaccines after prime and boost, similar to other SARS-CoV-2 vaccines (18, 60). While this finding may be related to VRP vaccine dose, our data also suggest that different sarbecoviruses may focus neutralizing antibody responses to different sites within S1, potentially complicating universal vaccine platforms focused exclusively on the RBD, especially when applied to outbred populations, like the human population (65, 66).

Although heterologous spike vaccines failed to elicit cross neutralizing antibodies against SARS-CoV-2 and still allowed infection in the lungs, these vaccines reduced viral loads in the lungs and provided partial protection from SARS-CoV-2 disease in *in vivo*. A similar phenotype, mediated by coronavirus nucleocapsid-based vaccines that stimulate T cells, has been reported following SARS-CoV and MERS-CoV challenge (59). While our data does not explicitly rule out a contribution of T cells in mediating protection after VRP vaccination, passive antibody transfer, systems serology, and vaccine studies in wild-type versus FcR deficient mice mechanistically link these non-neutralizing antibody functions as strong drivers of cross protection

In our model, cross-protection was highly clade dependent, as clade 1b and clade 2 VRP spikes protected with higher efficacy against SARS-CoV-2 disease than clade 1a VRP spikes. Clade 2 HKU3 contains as much antigenic diversity with the SARS-CoV-2 spike as clade 1a WIV1. However, the VRP HKU3 spike elicited near-complete protection from SARS-CoV-2 MA10 disease while the VRP WIV1 spike did not. This clade-dependent protection suggests that specific domain conservation, rather than overall sequence homology, drives the development of protective antibodies in our model. Additionally, we found that VRP SARS-CoV-2 spike vaccination, while unable to prevent infection, provided partial protection against disease induction by the heterologous bat virus, HKU3-SRBD MA. This result aligns with current data regarding spike-based vaccine efficacy against SARS-CoV-2 variants in the human population; where currently approved vaccines may not prevent variant infection in all cases but significantly reduce disease severity and death (67–70). Our model noted no cross protection following contemporary human coronavirus spike vaccinations against SARS-CoV-2. While contrary to some earlier correlative studies (22, 71–74), these differences may reflect repeat group 1A/2B human β-coronavirus infections, which might result in more cross protective humoral responses, highlighting an area of future investigation. Overall, our results indicate that when faced with

492 future sarbecovirus emergence events, cross protection from vaccine-mediated SARS-CoV-2
493 immunity has the potential to reduce disease severity or breadth of transmission. Still, this
494 protection is less likely to extend beyond the sarbecovirus subgenus.

495 There is increasing evidence of a potential role for non-neutralizing antibodies in long-term
496 SARS-CoV-2 vaccine protection, especially against VOC (39, 58, 75). Consistent with these
497 data, while heterologous antibodies elicited by VRP 3526-delivered sarbecovirus spikes did not
498 neutralize SARS-CoV-2, we detected and characterized cross-protective non-neutralizing
499 antibody activity through passive transfer experiments and systems serology. Our data
500 highlights non-neutralizing antibodies as correlates of heterologous vaccine-mediated protection
501 in an FcR-dependent manner. Furthermore, we detected strong FcR stimulation by antibodies
502 that recognized the SARS-CoV-2 spike as well as the S1 and S2 regions, especially the heptad
503 repeat 1 (HR1) region of S2, from the heterologous vaccines. Sarbecovirus strain variation-
504 dependent diversity of response in addition to the many instances of correlated stimulus
505 supports the hypothesis that the non-neutralizing cross protection may also be a function of the
506 cumulative effect of epitope conservation rather than driven by single or few broadly cross-
507 protective epitopes that are conserved across β-coronaviruses (76). Thus, Fc-effector immunity
508 may depend upon the number and quality of cross binding epitopes as well as the abundance of
509 cross-reactive antibodies, coupled with the types of FcR/effector mediated phenotypes.

510 Further supporting our results, we found that both homologous and heterologous protection was
511 less robust in aged animals, consistent with existing work (44, 51). Notably, age related waning
512 of FcR effector functions is thought to impact both vaccine efficacy and infection response (77–
513 79). Notably, neutrophil responses wane in aged populations and become dysregulated after
514 pulmonary infection (79). Additionally, overall effector cell function (e.g. infected cell killing)
515 becomes impaired with increased age (77, 78). Thus, as a function of increasing virus challenge
516 dose in aged animals, increased VRP sarbecovirus spike vaccine failure is consistent with
517 reduced FcR mediated protection, a prospect that will need to be carefully investigated in future
518 vaccine studies focused on the elderly.

519 While this work has shown that the VRP platform is a valuable experimental platform for
520 studying cross-protective coronavirus immunity, especially regarding non-neutralizing antibody
521 responses, the study design also highlights many areas for further investigation. The same
522 susceptibility loci appear to regulate sarbecovirus pathogenesis in mice and humans (53), and
523 the mouse model reproduces key aspects of acute and chronic SARS-CoV-2 induced disease
524 (42, 43). Furthermore, mouse models of SARS-CoV-2 disease have proven to be robust

platforms for predicting SARS-CoV-2 vaccine performance in humans (53, 80–82) and the alphavirus replicon strategy has shown utility as a vaccine platform (83–86). However, systems serology responses following alphavirus vaccination in humans have not been reported, including any reporting on non-neutralizing antibody functional activity. This study is the first that clearly implicated FcR-mediated protection following alphavirus VRP vaccination in any species as well as the first to directly correlate the FcR mechanism of cross-protection to disease outcome. However, our data was drawn from a limited sample size for correlation to disease (n = 4), prompting a need for further mechanistic investigation. Still, detailed systems serology studies have also suggested a robust correlative role for FcR-mediated protection after mRNA vaccination and the durability of protection when compared to prior infection (39). Additionally, FcR mechanisms of protection have been implicated in HIV vaccination (45), influenza vaccination (87–89), and DENV prior infection (90).

Although speculative, the results identified here may likely be relevant to understanding the mechanisms that promote vaccine-induced SARS-CoV-2 immunity in humans, as also evidenced by the fact that a recombinant SARS-CoV-2 RBD protein vaccine conferred cross protection in the absence of a potent cross neutralizing antibody response (91). However, most vaccine designs have not been tailored to maximize protective FcR effector functions despite clear animal model studies that have demonstrated that specific activation of distinct FcγR-mediated pathways significantly improves antibody-mediated protection as well as sustained and robust immune responses (39, 92–94). In addition, the exact antibodies and epitopes that contribute to cross protection via FcR mediated activities remain unclear, but obviously would help guide future pan-coronavirus therapeutic development including both monoclonal antibody treatment and vaccines. This is especially interesting in the unique case of cross-protection we observed with VRP HKU3 S. Investigating epitope conservation, in this case, may identify novel spike epitopes that contribute to broad cross-protection. For example, our work would propose that a pan-sarbecovirus vaccine would benefit from inclusion of the HR1 spike subdomain to induce cross-protective FcR effector responses. These studies also suggest that the VRP platform represents a valuable system both for human vaccine delivery and for dissecting the aspects of vaccine-induced immunity that mediate protection. It will be essential to determine whether these results extend beyond standard inbred mouse strains by testing their impact in outbred populations, such as the Collaborative Cross (95, 96), or other models of SARS-CoV-2-induced disease like non-human primates to further probe the mechanisms of cross protection discussed.

As SARS-CoV-2 is the second sarbecovirus to emerge in the 21st century, other coronaviruses will likely arise in the future, including those with similar or different spike sequences to those examined in this study (e.g. SHC014 and WIV1) (4) and others (e.g. swine acute diarrhea syndrome (SADS) coronavirus) (97). Therefore, the inclusion of non-neutralizing, cross-protective epitopes informed by the results of our study may shift vaccine development toward a more comprehensive, cross-protective formulation that prevents life-threatening sarbecovirus disease and provide new insights for vaccine design against other highly heterogeneous RNA virus families, including *Coronaviridae*.

FIGURES

Table 1. Amino acid percent similarity | patristic phylogenetic distance of sarbecovirus spike proteins

	SARS-CoV-2	RaTG13	SARS-CoV	SHC014	WIV1
RaTG13	97.4 | 0.023				
SARS-CoV	75.6 | 0.248	76.2 | 0.247			
SHC014	76.8 | 0.246	77.0 | 0.245	90.0 | 0.099		
WIV1	76.5 | 0.233	77.0 | 0.232	92.3 | 0.086	97.1 | 0.030	
HKU3	75.8 | 0.248	76.0 | 0.247	78.1 | 0.225	78.8 | 0.223	78.8 | 0.210

AA % similarity | patristic phylogenetic distance

Figure 1. Venezuelan Equine Encephalitis Virus Replicon Particle VRP3526 for high-titer vaccinations. A. Fragmented RNA-based assembly scheme of VRP3526 particles. **B.** Phylogenetic relationships of CoV spike proteins that were used in this study, including common cold CoVs (green) and prepandemic/epidemic CoVs (red). Of the β-coronaviruses, we generated spike proteins for both group 2A (HKU1) and 2B viruses. Of the group 2B viruses, we generated spike proteins for clade 1a (SARS-CoV, SHC014, WIV1), 2 (HKU3), and 1b (SARS-CoV-2, RaTG13) viruses. Tree generated from an amino acid multiple sequence alignment using Maximum Likelihood in Geneious Prime. **C.** VRP3526 titers obtained in this study. Dashed line denotes minimum titer required for vaccination at $2x10^4$ VRP in a 10 µl footpad inoculation. **D.** Immunofluorescent staining at 40x magnification for VEE non-structural proteins (top) and

SARS-CoV-2 spike S2 domain (middle) in Vero E6 cells infected with VRPs expressing the spike proteins used in this study.

Figure 2. VRP sarbecovirus spike vaccines elicit a cross-protective immune response against SARS-CoV-2. A SARS-CoV-2 lung titer calculated via plaque assay on days 2 and 5 post infection. Samples that fell below the limit of detection (dotted line) were set to 25 PFU/mL. **B.** Area under the curve (AUC) of lung function metrics of airflow resistance (PenH, right) and bronchoconstriction (Rpef, left). Lung function was measured by BUXCO whole body plethysmography systems one each experimental day, AUC calculated for time course of each mouse. **C-E.** Body weights calculated after infection of 10^4 PFU SARS-CoV-2 intranasally through the duration of the experiment on animals vaccinated with clade 1b (**C**), 2 (**D**), and 1a (**E**) sarbecovirus spike proteins. Reported as percent of starting weight. Horizontal line indicates 20% body weight lost and animal care humane endpoint. **F.** Semi-quantitative gross lung discoloration (GLD) scoring, **G.** Diffuse alveolar damage (DAD) scoring, and **H.** acute lung injury (ALI) scoring upon tissue harvest at day 5 post infection. **I.** Hematoxylin and eosin stained sections of lungs from vaccinated mice harvested day 5 post infection. Black arrow – hyaline membrane, blue arrow – neutrophil infiltrate, red arrow – proteinaceous debris. Top – 100x magnification, 100 μm scale. Bottom – 400x magnification, 50 μm scale. * $p < 0.05$, ** $p < 0.01$, *** $p < 0.001$, **** $p < 0.0001$ after statistical testing described in methods.

Figure 3. VRP Spike protects from lethal infection in vulnerable aged mice. Old mice (12 months) were challenged with 10^3 PFU SARS-CoV-2 MA10 intranasally unless otherwise noted. **A-C.** Body weights calculated through the duration of the experiment on animals vaccinated with clade 1b (**A**), 2 (**B**), and 1a (**C**) sarbecovirus spike proteins. Reported as percent of starting weight. Horizontal line indicates 20% body weight lost and animal care humane endpoint. **D.** GLD scoring upon tissue harvest. **E.** SARS-CoV-2 lung titer calculated via plaque assay. Samples that fell below the limit of detection (dotted line) were set to 25 PFU/mL. **F**. Area under the curve (AUC) of lung function metrics of airflow resistance (PenH, right) and bronchoconstriction (Rpef, left). Lung function was measured by BUXCO whole body plethysmography systems one each experimental day, AUC calculated for time course of each mouse. **G.** Survival of vaccinated animals when challenged with 10^4 PFU SARS-CoV-2 MA10 intranasally. * $p < 0.05$, ** $p < 0.01$, *** $p < 0.001$, **** $p < 0.0001$ after statistical testing described in methods.

Figure 4. **VRP SARS-CoV-2 spike vaccination protects against heterologous challenge.** Young mice (16-18 weeks) were challenged with 10^5 PFU HKU3/sRBD MA (**A**-**C**) or old mice

(12 months) were challenged with 10^5 PFU SARS-CoV-2 MA10 containing the omicron variant spike (**D**-**F**) intranasally. **A.** Body weights calculated through the duration of the experiment on animals vaccinated with SARS-CoV-2 or HKU3 spike proteins, or vectored GFP. **B.** Semi-quantitative macroscopic lung discoloration scoring upon tissue harvest. **C.** HKU3 lung titer calculated via plaque assay. * $p < 0.05$, ** $p < 0.01$, *** $p < 0.001$, **** $p < 0.0001$ after statistical testing described in methods. Body weights reported as percent of starting weight where horizontal line indicates 20% body weight lost and animal care humane endpoint. Titer samples that fell below the limit of detection (dotted line) were set to 25 PFU/mL.

Figure 5. Characterizing the antibody response through systems serology and functional assays. A. SARS-CoV-2 spike (left), receptor binding domain (middle), and N-terminal domain (right) binding IgG quantified by ELISA. Titers calculated via area under the curve (AUC). **B.** SARS-CoV-2 spike binding IgG2a titers plotted against IgG1 titers. Titer calculated by gMFI. **C.** SARS-CoV-2 spike (left), S1 (middle), and S2 (right) binding IgG2a titer calculated by gMFI via Luminex bead assay. * $p < 0.05$, ** $p < 0.01$, *** $p < 0.001$, **** $p < 0.0001$ after statistical testing described in methods, comparing each vaccine group to GFP. **D.** SARS-CoV-2 neutralization IC_{50} values calculated as the serum dilution that achieved 50% neutralization in a live-virus neutralization assay. **E.** Domain-specific IC_{50} values measured by live-virus neutralization assay against different SARS-CoV-2 spike domains on a heterologous virus backbone (SHC014). **F.** SHC014 neutralization IC_{50} values of serum from vaccinated animals. **G.** Domain-specific IC_{50} values measured by live-virus neutralization assay against different SARS-CoV-2 spike domains on the SHC014 backbone. IC_{50} for samples that fell below the limit of detection (dotted line) were set to 10. **H.** A scores plot representing the baseline (blue) and post-boost (red) vaccine immunoglobulin and functional profile distribution for all vaccinated animals tested, clustered via PLSDA (partial least squares discriminant analysis). **I.** VIP score of most influential features, representing the total distance from the center of the scores plot, as determined by PLSDA of immunoglobulin and functional profiles. **J.** A scores plot representing the baseline (blue) and post-boost (red) vaccine Fc receptor stimulation and functional profile distribution for all vaccinated animals tested, clustered via PLSDA (partial least squares discriminant analysis). **K.** VIP score of most influential features, representing the total distance from the center of the scores plot, as determined by PLSDA of Fc receptor stimulation and functional profiles.

Figure 6. Non-neutralizing antibodies mediate protection *in vivo* through Fc function. A. Pearson's correlation matrices were constructed of the systems serology assays for each VRP vaccination group (**Supplemental data**). VRP vaccine groups with strong correlations (0.7 – 1)

between two assay results are listed in the table. **B.** FcgR4 stimulation against the SARS-2 spike (left), S1 (middle), and S2 (right) **C.** Phagocytic score of antibody-dependent neutrophil phagocytosis (ADNP) and **D.** Phagocytic score of antibody-dependent cellular phagocytosis (ADCP). **E.** body weights, **F.** GLD scores day 5 post infection, and **G.** SARS-2 lung titer in naïve mice after passive transfer of serum from vaccinated animals followed by intranasal infection of 10^4 PFU SARS-2. **H.** Body weights, **I.** GLD scores day 5 post infection, and **J**. SARS-2 lung titer of young Fc receptor knockout BALB/c mice that were vaccinated with a sarbecovirus spike protein prior to infection with 10^4 PFU SARS-2 intranasally. **K.** Body weights, **L.** GLD scores day 5 post infection, and **M.** SARS-CoV-2 lung titer of young Fc receptor knockout BALB/c mice that received prophylactic administration of serum from vaccinated wild-type BALB/c mice prior to infection with 10^3 PFU SARS-CoV-2 intranasally. * $p < 0.05$, ** $p < 0.01$, *** $p < 0.001$, **** $p < 0.0001$ after statistical testing described in methods. Body weights reported as percent of starting weight where horizontal line indicates 20% body weight lost and animal care humane endpoint. Titer samples that fell below the limit of detection (dotted line) were set to 25 PFU/mL.

Figure S1. Pairwise sequence alignments of sarbecovirus spike proteins to the SARS-CoV-2 spike protein. Global alignments constructed with Blosum62 matrix with free end gaps in Geneious Prime. Alignments of SARS-CoV-2 to **A.** RaTG13 **B.** HKU3 **C.** SARS **D.** WIV1 and **E.** SHC014. Blue – NTD, red – RBD, green – S2.

Figure S2. VRP-vectored endemic coronavirus spike protein vaccinations do not protect against severe SARS-CoV-2 disease in young BALB/c mice. A. Body weights and **B**. lung titer calculated for animals vaccinated with spike proteins from contemporary human CoVs. **C.** Percent survival of animals vaccinated with each spike protein. * $p < 0.05$, ** $p < 0.01$, *** $p < 0.001$, **** $p < 0.0001$.

Figure S3. Lung cytokine signatures in VRP-vaccinated mice. Measured by BioPlex, cytokine signatures associated with immune responses were measured on days 2 and 5 post-infection with SARS-CoV-2 MA10. * $p < 0.05$, ** $p < 0.01$, *** $p < 0.001$, **** $p < 0.0001$.

Figure S4. VRP-vectored cross-protection wanes in aged animals with high dose lethal challenge. Old mice (12 months) were challenged with 10^4 PFU SARS-CoV-2 MA10 intranasally. **A.** Body weights calculated through the duration of the experiment on animals vaccinated with sarbecovirus spike proteins. Reported as percent of starting weight. **B.** Semi-quantitative macroscopic lung discoloration scoring upon tissue harvest. **C.** SARS-CoV-2 lung titer calculated via plaque assay. * $p < 0.05$, ** $p < 0.01$, *** $p < 0.001$, **** $p < 0.0001$. Body weights reported as percent of starting weight where horizontal line indicates 20% body weight

lost and animal care humane endpoint. Titer samples that fell below the limit of detection (dotted line) were set to 25 PFU/mL.

Figure S5. Systems serology reveals novel mechanisms of protection. The geometric mean fluorescent intensity (gMFI) value of each systems serology assay for a given serum sample plotted on a heatmap after log transformation.

Figure S6. Correlation matrix of all systems serology metrics tested. Pearson's correlation coefficient calculated for each pair of systems serology assay for the listed set of post-boost serum samples. **A.** Full data set of metrics for all samples. **B.** VRP GFP **C.** VRP SARS-CoV-2 spike **D.** VRP RaTG13 spike **E.** VRP HKU3 spike **F.** VRP SARS-CoV spike **G.** VRP WIV1 spike **H.** VRP SHC014 spike post boost serum samples tested.

Figure S7. Identification of likely cross-protection drivers. A. Heatmap identifying IgG2a peptide recognition clusters. **B.** Background-subtracted IgG2a peptide binding within S2 **C.** VRP vaccine groups with strong correlations between disease (AUC bodyweight curve) and antibody factors as identified via Pearson's correlation matrices. **D.** Multiple sequence alignments of S2 subdomains.

METHODS

Biosafety and institutional approval

All experiments were conducted after approval from the UNC Chapel Hill Institutional Biosafety Committee and Institutional Animal Care and Use Committee according to guidelines outlined by the Association for the Assessment and Accreditation of Laboratory Animal Care and the US Department of Agriculture. All vaccinations were performed at ABSL2 while all infections and downstream assays were performed at ABSL3 in accordance with Environmental Health and Safety. All work was performed with approved standard operating procedures and safety conditions for SARS-CoV-2. Our institutional ABSL3 facilities have been designed to conform to the safety requirements recommended by Biosafety in Microbiological and Biomedical Laboratories (BMBL), the US Department of Health and Human Services, the Public Health Service, the Centers for Disease Control and Prevention (CDC), and the National Institutes of Health (NIH). Laboratory safety plans have been submitted, and the facility has been approved for use by the UNC Department of Environmental Health and Safety (EHS) and the CDC.

Cell Lines and viruses

All cell lines and viruses were confirmed mycoplasma-negative. All viruses used were subjected to next-generation sequencing prior to use. Vero E6 cells were maintained in Dulbecco's Modified Eagle's Medium (DMEM) supplemented with 5% FBS and anti/anti. Baby Hamster Kidney (BHK21) cells were maintained in α -MEM supplemented with 10% fetal bovine serum, L-glutamine, and 10% tryptose phosphate broth. Mouse adapted SARS-CoV-2 MA10(42) and SARS-CoV-2 nanoLuciferase reporter viruses were developed based on the SARS-CoV-2 WA1 reference strain (98) and propagated from a cDNA molecular clone as previously described. Mouse adapted bat virus HKU3 was generated from a cDNA molecular clone (11, 53) and mutations were inserted that cause pathogenesis in mice. To generate the SARS-CoV-2 spike domain panel, the backbone sequence from bat virus SHC014 (4) was used. SHC014 spike sequences were replaced with corresponding fragments of the sequence encoding SARS-CoV-2 spike segments (RBD, RBD+, NTD, RBD-NTD, S1) and viruses were generated from the cDNA clone.

VEE VRP3526 vaccine preparation

The sequence encoding CoV spike proteins (below) were cloned into the pVR21 vector containing Venezuelan equine encephalitis virus strain 3526 non-structural proteins. RNA from template pVR21 constructs and VEE 3526 helper constructs encoding glycoprotein and capsid proteins was transcribed using Invitrogen T7 mMessage mMachine *in vitro* transcription kit. Purified RNA was electroporated into BHK21 cells in the ratio of 2:1:1 pVR21 construct : VEE 3526 glycoprotein : capsid. Supernatant was harvested and purified 24 hours post-electroporation and ultracentrifuge concentrated through sucrose cushion. VRP titers were determined through immunofluorescent staining to detect VEE-associated proteins. All VRPs were confirmed to not cause cytopathic effect in cell culture before administration to mice.

Spike sequences used to construct VRP vaccines:

SARS-CoV-2	MT020880.1	HKU3	FJ211859.1
RaTG13	MN996532.2	NL63	AY567487.2
SARS-CoV	AY278741	OC43	UDM84911.1
SHC014	KC881005.1	229E	KY621348.1
WIV1	KC881007.1	HKU1	HM034837.1

Mice, vaccination, and infection

BALB/cAnNHsd were obtained from Envigo (strain 047) and delivered at either 8-10 weeks (young) or 11-12 months (old) for vaccination and housed in groups under standard conditions. Mice were vaccinated with $2x10^4$ VRP in a 10 µl phosphate-buffered saline footpad inoculation and boosted with the same dose 3 weeks post-prime. Baseline, pre-boost, and pre-challenge serum was collected via submandibular bleed. Four weeks post-boost, mice were infected with 10^3 or 10^4 (where specified) PFU SARS-CoV-2 MA10 or 10^5 PFU HKU3 MA-SRBD in 50 µl PBS intranasally under ketamine-xylasine anesthesia. The challenge doses were at least one log higher than the suspect infectious dose in humans (99). For adoptive and passive transfer experiments, 200 µl serum from vaccinated mice was transferred to naïve mice via intraperitoneal injection 24 hours prior to challenge. Mice were weighed daily through the course of infection, and a subset's respiratory function was tracked daily using whole body plethysmography (48). Mice were euthanized at 2 and 5 days post infection via isoflurane overdose. FcR-knockout mice were obtained from Taconic (Model 584), on a BALB/cAnNTac background delivered at 6-10 weeks old due to strain availability. The relevant infectious challenge dose for this strain was determined to be 10^3 PFU SARS-CoV-2 MA10 due to strain-specificities, and mice were infected and monitored as described above.

Mouse tissue collection and analysis

After euthanasia, blood was collected into phase separation tubes by cardiocentesis or severing the vena cava and allowed to clot before centrifugation to separate serum. Lungs were scorerd for gross discoloration, indicating congestion and/or hemorrhage, based on a semi-quantitative scale of mild to severe discoloration covering 0 to 100% of the lung surface. The left lung was collected and injected with 10% neutral buffered formalin to expand airways before storage in fixative for 7 days before histopathological processing. Of the right lung lobes, the inferior lobe was collected in ~1 mL TRIzol reagent with glass beads and the superior lobe was collected in ~1 mL phosphate buffered saline with glass beads. Both inferior and superior lobes were homogenized in a MagnaLyser and debris was pelleted. Virus in the lungs was quantified from the superior lobe via plaque assay. Briefly, virus was serial diluted and inoculated onto confluent monolayers of Vero E6 cells, followed by agarose overlay. Plaques were visualized on day 2 post infection via staining with neutral red dye. Lung cytokines were quantified from the superior lobe using the Bio-Plex Pro Mouse Cytokine 23-Plex Immunoassay. RNA from the inferior lobe was reserved for additional downstream assays.

Neutralization assays

A serial dilution (1:20 initially, followed by a 3-fold dilution) of pre-challenge serum was incubated in a 1:1 ratio with SARS-CoV-2-nLuc (98) to result in 800 PFU virus per well. Serum-virus complexes were incubated at 37C with 5% CO2 for 1 hour. Following incubation, serum-virus complexes were added to a confluent monolayer of Vero E6 cells and incubated for 48 hours at 37C with 5% CO_2. After incubation, luciferase activity was measured with the Nano-Glo Luciferase Assay System (Promega) according to the manufacturer specifications. Neutralization titers (EC50) were defined as the dilution at which a 50% reduction in RLU was observed relative to the virus (no antibody) control.

Systems Serology

SARS-CoV-2 and other sarbecovirus and control antigens were resuspended in water to a final concentration of 0.5 mg/mL and linked to magnetic Luminex beads (Luminex Corp, TX, USA) through carbodiimide NHS ester linkages. Specific antigens were coupled to individual bead regions. Biotinylation of antigens were done using the NHS-Sulfo-LC-LC kit, and excess biotin was removed using Zebra-Spin desalting and size exclusion columns. Antigen coupled beads were then incubated with serum at various dilutions (1:100 for IgG2a, IgG2b, IgG3, IgM, 1:200 for IgG1, and 1:750 for Fcγ-receptor binding) in a 384-well plate (Greiner, Germany) overnight at 4°C. Unbound material was washed and detection of isotypes and subclasses were done using PE-conjugated anti-IgG1, -IgG2a, -IgG2b, -IgG3, -IgM. PE-Streptavidin (Agilent Technologies, CA, USA) was coupled to recombinant and biotinylated mouse FcγR2b, FcγR3, and FcγR4A at a 1:1000 dilution. Secondary detection was done at room temperature for 1 hour, and unbound material was removed by washing. Relative binding per antigen was determined on an IQue Screener PLUS cytometer (IntelliCyt).

Antibody-dependent cellular phagocytosis (ADCP) and neutrophil phagocytosis (ADNP) assays were done as previously described (100). Mouse serum was incubated with cultured monocytes or primary neutrophils at a concentration of 1:100 on preformed immune complexes on fluorescent neutravidin microspheres. Cells were fixed with 4% paraformaldehyde (PFA) and identified by gating on microsphere-positive cells. Phagocytic score was quantified by the (percentage of microsphere-positive cells) x (MFI of microsphere-positive cells) divided by 100000. Antibody-dependent complement deposition (ADCD) was done as previously described (101). Relative complement deposition was quantified through flow cytometry, as measured by fluorescein-conjugated goat IgG that targets the guinea pig complement C3b.

Correlations between Fab, FcR, and functional assays were done using GraphPad Prism using Spearman's coefficients. Statistical significance, as defined by $p < 0.05$, was corrected for

multiple comparisons using Benjamini-Hochberg correction. Other analyses such as PLS-DA were done on R using the systemsseRology pipeline available on GitHub (GitHub - LoosC/systemsseRology: Machine learning tools (for the analysis of systems serology data) are also available. Each assay contained pre-immune and post-vaccination sera, as well as PBS controls to account for batch effects. All other calculations are described below.

Key reagents used in systems serology assays

Anti-mouse IgG1-PE	Southern Biotech	1144-09
Anti-mouse IgG2a-PE	Southern Biotech	1155-09L
Anti-mouse IgG2b-PE	Southern Biotech	1186-09L
Anti-mouse IgG3-PE	Southern Biotech	1191-09L
Anti-mouse IgM-PE	Southern Biotech	1021-09
Anti-CD66b Pac Blue	BioLegend	305112
Anti-CD3	BD Biosciences	558117
Anti-CD16	BD Biosciences	557758
Anti-CCL4	BD Biosciences	550078
Anti-C3b	MP Biomed	855385
SARS-CoV-2 WT Spike	Sino Biological	40589-V08H4
SARS-CoV-2 D614G Spike	Sino Biological	40589-V08H8
SARS-CoV-2 WT S1 Domain	Sino Biological	40591-V08H
SARS-CoV-2 WT Receptor Binding Domain (RBD)	Sino Biological	40592-V08H
SARS-CoV-2 WT S2 Domain	Sino Biological	40590-V08B
SARS-CoV-2 WT N-terminal Domain	Sino Biological	40591-V49H
SARS-CoV-2 Alpha Variant S	Sino Biological	40589-V08B6
SARS-CoV-2 Beta Variant S	Sino Biological	40589-V08B7
SARS-CoV-2 Delta Variant S	Sino Biological	40589-V08B16
SARS-CoV-2 Omicron Variant S	Sino Biological	40589-V08H26
Human Coronavirus OC43 S	Sino Biological	40607-V08B
Human CoV HKU1 S (isolate N5)	Sino Biological	40606-V08B
Human Cytomegalovirus (HCMV) Glycoprotein B (gB)	Sino Biological	10202-V08H1
Human Coronavirus 229E Spike	Sino Biological	40605-V08B
SARS-CoV-1 Spike	Sino Biological	40634-V08B
PE-Streptavidin	Agilent Technologies	PB32-10
Guinea Pig Complement	Cedarlane	CL4051
Protein Transport Inhibitor	BD Biosciences	554724
Brefeldin-A	Sigma	B7651
NHS-Sulfo-LC-LC Kit	ThermoFisher	21435
Zebra-Spin Desalting and Chromatography Columns	ThermoFisher	89882
Fix & Perm Cell Permeabilization Kit	ThermoFisher	GAS002S-100
R Studio V 1.4.1103	RStudio, PBC	Open Source
GraphPad Prism	GraphPad Software, LLC	Ragon Site License
FlowJo V. 10.8	FlowJo, LLC	www.flowjo.com/so

		lutions/flowjo/downloads
iQue Forecyt	Sartorius	60028
iQue Screener Plus	Intellicyt/Sartorius	11811
384-well HydroSpeed Plate Washer	Tecan	30190112
MagPlex Microspheres	Luminex MFG	MC12001-01 (Cataloged by region)
Green Fluorescent Neutravidin Microspheres	ThermoFisher	F8776
Red Fluorescent Neutravidin Microspheres	ThermoFisher	F8775

807

808 **Enzyme-Linked Immunosorbent Assay**

809 *Full-length spike protein ELISA titer*

810 All serum samples tested by ELISA assay were heat-inactivated at 56°C for 30 min to reduce
811 risk from possible residual virus in serum. ELISA binding titer for full-length spike protein was
812 measured as described before (102). Essentially, full-length spike protein at 2 µg/mL in Tris-
813 Buffered Saline (TBS) pH 7.4 was coated in the 96-well microtiter plate for 1 hour at 37°C. The
814 wells were blocked with 3% milk in TBS containing 0.05% Tween 20 (TBST) for 1 hour, then
815 serially diluted serum samples were added (1:100 – 1:24,300) to the wells and incubated for an
816 additional hour at 37°C. The plate was washed three times using wash buffer (TBS containing
817 0.2% Tween 20), then respective goat anti-mouse IgG (Catalog # A16072), IgG1 (Catalog #
818 PA1-74421), or IgG2A (Catalog # M32207) was added at 1:2000 and incubated for 1 hour at
819 37°C. The plate was washed three times using wash buffer, then 3,3′,5,5′-Tetramethylbenzidine
820 (TMB) Liquid Substrate (Sigma-Aldrich) was added to the plate, and absorbance was measured
821 at 450 nm using a plate reader (Molecular Devices SpectraMax ABS Plus Absorbance ELISA
822 Microplate Reader) after stopping the reaction with 1 N HCl.

823 *RBD or NTD ELISA titer*

824 All serum samples tested by ELISA assay were heat-inactivated at 56°C for 30 min to reduce
825 risk from possible residual virus in serum. ELISA binding titer for Spike RBD or NTD was
826 measured as described above with minor modifications. 96-well microtiter plate was coated with
827 Streptavidin (Invitrogen) at 4 µg/mL in TBS pH 7.4 for 1 hour at 37°C. The wells were blocked
828 with 1:1 Non-Animal Protein-BLOCKER™ (G-Biosciences) in TBS for 1 hour. Biotinylated spike
829 RBD or NTD antigen (1 µg/ml) was captured onto the streptavidin-coated wells, then serially
830 diluted serum samples (1:100 – 1:24,300) were added to the wells and incubated for 1 hour at

37°C. The plate was washed three times using wash buffer (TBS containing 0.2% Tween 20), then goat anti-mouse IgG (Catalog # A16072) was added at 1:2000 and incubated for 1 hour at 37°C. The plate was washed three times using wash buffer, then 3,3′,5,5′-Tetramethylbenzidine (TMB) Liquid Substrate (Sigma-Aldrich) was added to the plate, and absorbance was measured at 450 nm using a plate reader (Molecular Devices SpectraMax ABS Plus Absorbance ELISA Microplate Reader) after stopping the reaction with 1 N HCl.

Statistical testing

All statistical analyses were conducted in GraphPad PRISM 9. To assess the statistical significance of weight loss, significance was calculated by two-way ANOVA comparing each spike vaccinated group to the GFP control. In cases where mortality was observed, significance was calculated via Mixed-effects analysis The significance of virus and antibody titers was calculated via one-way ANOVA comparing each spike vaccinated group to the GFP control. To assess the significance of lung discoloration and histopathological lung damage scoring, significance was calculated via Brown-Forsythe and Welch's ANOVA. In all cases, testing was corrected for multiple comparisons using Dunnett's multiple comparisons test, Dunnett's T3 test when total samples <50. Significance reported as * $p < 0.05$, ** $p < 0.01$, *** $p < 0.001$, **** $p < 0.0001$.

ACKNOWLEDGEMENTS

GA and the Systems Serology Lab at Ragon are supported by Mark and Lisa Schwartz, Terry and Susan Ragon, and the SAMANA Kay MGH Research Scholars award. GA and the Systems Serology Lab also receives funding from the Massachusetts Consortium on Pathogen Readiness (MassCPR), the Gates Global Health Vaccine Accelerator Platform, and the NIH (3R37AI080289-11S1, R01AI146785, U19AI42790-01, U19AI135995-02, U19AI42790-01, P01AI165072, U01CA260476 – 01, CIVIC75N93019C00052). VKB receives funding from NIH grant K01OD026529. RSB and MTH receive funding from NIH grant P01AI158571. RSB receives funding from NIH/NCI North Carolina Seronet Center for Excellence grant U54 CA260543. LEA is supported in part by NIH 2T32AI007419-26 Molecular Biology of Viral Diseases Predoctoral Training Grant. This project was also supported in part by the North Carolina Policy Collaboratory at the University of North Carolina at Chapel Hill with funding from the North Carolina Coronavirus Relief Fund established and appropriated by the North Carolina General Assembly. We would like to also thank Sharon Taft-Benz for valuable input coordinating, directing, and managing studies in ABSL3 facilities.

DISCLOSURES

GA is a founder/equity holder in Seroymx Systems and Leyden Labs. GA has served as a scientific advisor for Sanofi Vaccines. GA has collaborative agreements with GSK, Merck, Abbvie, Sanofi, Medicago, BioNtech, Moderna, BMS, Novavax, SK Biosciences, Gilead, and Sanaria.

REFERENCES

1. P. A. Rota, *et al.*, Characterization of a novel coronavirus associated with severe acute respiratory syndrome. *Science* **300**, 1394–1399 (2003).

2. P. Zhou, *et al.*, A pneumonia outbreak associated with a new coronavirus of probable bat origin. *Nature* **579**, 270–273 (2020).

3. V. D. Menachery, *et al.*, SARS-like WIV1-CoV poised for human emergence. *Proceedings of the National Academy of Sciences* **113**, 3048–3053 (2016).

4. V. D. Menachery, *et al.*, A SARS-like cluster of circulating bat coronaviruses shows potential for human emergence. *Nature Medicine* **21**, 1508–1513 (2015).

5. S. K. P. Lau, *et al.*, Severe acute respiratory syndrome coronavirus-like virus in Chinese horseshoe bats. *PNAS* **102**, 14040–14045 (2005).

6. W. Li, *et al.*, Bats Are Natural Reservoirs of SARS-Like Coronaviruses. *Science* **310**, 676–679 (2005).

7. S. Temmam, *et al.*, Bat coronaviruses related to SARS-CoV-2 and infectious for human cells. *Nature* (2022) https:/doi.org/10.1038/s41586-022-04532-4 (February 16, 2022).

8. R. Arya, *et al.*, Structural insights into SARS-CoV-2 proteins. *J Mol Biol* **433**, 166725 (2021).

9. L. E. Adams, *et al.*, Critical ACE2 Determinants of SARS-CoV-2 and Group 2B Coronavirus Infection and Replication. *mBio* **12** (2021).

10. Y. Wan, J. Shang, R. Graham, R. S. Baric, F. Li, Receptor Recognition by the Novel Coronavirus from Wuhan: an Analysis Based on Decade-Long Structural Studies of SARS Coronavirus. *Journal of Virology* **94**, e00127-20 (2020).

11. M. M. Becker, *et al.*, Synthetic recombinant bat SARS-like coronavirus is infectious in cultured cells and in mice. *Proc Natl Acad Sci U S A* **105**, 19944–19949 (2008).

12. K. S. Corbett, *et al.*, SARS-CoV-2 mRNA vaccine design enabled by prototype pathogen preparedness. *Nature* **586**, 567–571 (2020).

13. D. Laczkó, *et al.*, A Single Immunization with Nucleoside-Modified mRNA Vaccines Elicits Strong Cellular and Humoral Immune Responses against SARS-CoV-2 in Mice. *Immunity* **53**, 724-732.e7 (2020).

14. J. Lu, *et al.*, A COVID-19 mRNA vaccine encoding SARS-CoV-2 virus-like particles induces a strong antiviral-like immune response in mice. *Cell Res* **30**, 936–939 (2020).

15. D. W. Hawman, *et al.*, SARS-CoV2 variant-specific replicating RNA vaccines protect from disease following challenge with heterologous variants of concern. *Elife* **11**, e75537 (2022).

16. J. H. Erasmus, *et al.*, An Alphavirus-derived replicon RNA vaccine induces SARS-CoV-2 neutralizing antibody and T cell responses in mice and nonhuman primates. *Sci Transl Med* **12**, eabc9396 (2020).

17. G. Palladino, *et al.*, Self-amplifying mRNA SARS-CoV-2 vaccines raise cross-reactive immune response to variants and prevent infection in animal models. *Molecular Therapy - Methods & Clinical Development* **25**, 225–235 (2022).

18. D. R. Martinez, *et al.*, Chimeric spike mRNA vaccines protect against Sarbecovirus challenge in mice. *Science* **373**, 991–998 (2021).

19. F. A. Olotu, K. F. Omolabi, M. E. S. Soliman, Leaving no stone unturned: Allosteric targeting of SARS-CoV-2 spike protein at putative druggable sites disrupts human angiotensin-converting enzyme interactions at the receptor binding domain. *Informatics in Medicine Unlocked* **21**, 100451 (2020).

20. M. A. Díaz-Salinas, *et al.*, Conformational dynamics and allosteric modulation of the SARS-CoV-2 spike. *eLife* **11**, e75433 (2022).

21. A. O. Hassan, *et al.*, A SARS-CoV-2 Infection Model in Mice Demonstrates Protection by Neutralizing Antibodies. *Cell* **182**, 744-753.e4 (2020).

22. J. Mateus, *et al.*, Selective and cross-reactive SARS-CoV-2 T cell epitopes in unexposed humans. *Science* **370**, 89–94 (2020).

23. Y. Zhu, *et al.*, Cross-reactive neutralization of SARS-CoV-2 by serum antibodies from recovered SARS patients and immunized animals. *Science Advances* **6**, eabc9999 (2020).

24. X. Xie, *et al.*, Neutralization of SARS-CoV-2 spike 69/70 deletion, E484K and N501Y variants by BNT162b2 vaccine-elicited sera. *Nat Med* **27**, 620–621 (2021).

25. C. G. Rappazzo, *et al.*, Broad and potent activity against SARS-like viruses by an engineered human monoclonal antibody. *Science* **371**, 823–829 (2021).

26. A. Nelde, *et al.*, SARS-CoV-2 T-cell epitopes define heterologous and COVID-19-induced T-cell recognition (2021) https:/doi.org/10.21203/rs.3.rs-35331/v1 (July 30, 2021).

27. L. Liu, *et al.*, Potent neutralizing antibodies against multiple epitopes on SARS-CoV-2 spike. *Nature* **584**, 450–456 (2020).

28. D. Pinto, *et al.*, Cross-neutralization of SARS-CoV-2 by a human monoclonal SARS-CoV antibody. *Nature* **583**, 290–295 (2020).

29. D. Li, *et al.*, In vitro and in vivo functions of SARS-CoV-2 infection-enhancing and neutralizing antibodies. *Cell*, S009286742100756X (2021).

30. D. Li, G. D. Sempowski, K. O. Saunders, P. Acharya, B. F. Haynes, SARS-CoV-2 Neutralizing Antibodies for COVID-19 Prevention and Treatment. *Annual Review of Medicine* **73**, null (2022).

31. J. R. R. Whittle, *et al.*, Broadly neutralizing human antibody that recognizes the receptor-binding pocket of influenza virus hemagglutinin. *Proc Natl Acad Sci U S A* **108**, 14216–14221 (2011).

32. Z. Wang, *et al.*, Conserved Neutralizing Epitopes on the N-Terminal Domain of Variant SARS-CoV-2 Spike Proteins. *bioRxiv*, 2022.02.01.478695 (2022).

33. K. M. Hastie, *et al.*, Defining variant-resistant epitopes targeted by SARS-CoV-2 antibodies: A global consortium study. *Science* **374**, 472–478 (2021).

34. D. R. Martinez, *et al.*, A broadly cross-reactive antibody neutralizes and protects against sarbecovirus challenge in mice. *Science Translational Medicine* (2021) https:/doi.org/10.1126/scitranslmed.abj7125 (January 18, 2022).

35. R. Yamin, *et al.*, Fc-engineered antibody therapeutics with improved anti-SARS-CoV-2 efficacy. *Nature*, 1–6 (2021).

36. A. Tauzin, *et al.*, A single dose of the SARS-CoV-2 vaccine BNT162b2 elicits Fc-mediated antibody effector functions and T cell responses. *Cell Host & Microbe* **29**, 1137-1150.e6 (2021).

37. Y. C. Bartsch, *et al.*, Humoral signatures of protective and pathological SARS-CoV-2 infection in children. *Nat Med* **27**, 454–462 (2021).

38. C. E. Z. Chan, *et al.*, The Fc-mediated effector functions of a potent SARS-CoV-2 neutralizing antibody, SC31, isolated from an early convalescent COVID-19 patient, are essential for the optimal therapeutic efficacy of the antibody. *PLOS ONE* **16**, e0253487 (2021).

39. P. Kaplonek, *et al.*, mRNA-1273 vaccine-induced antibodies maintain Fc effector functions across SARS-CoV-2 variants of concern. *Immunity* **55**, 355-365.e4 (2022).

40. P. Bruhns, F. Jönsson, Mouse and human FcR effector functions. *Immunol Rev* **268**, 25–51 (2015).

41. S. Agnihothram, *et al.*, Development of a Broadly Accessible Venezuelan Equine Encephalitis Virus Replicon Particle Vaccine Platform. *Journal of Virology* **92** (2018).

42. S. R. Leist, *et al.*, A Mouse-adapted SARS-CoV-2 induces Acute Lung Injury (ALI) and mortality in Standard Laboratory Mice. *Cell* **183**, 1070–1085 (2020).

43. K. H. Dinnon, *et al.*, A mouse-adapted model of SARS-CoV-2 to test COVID-19 countermeasures. *Nature* **586**, 560–566 (2020).

44. D. Deming, *et al.*, Vaccine Efficacy in Senescent Mice Challenged with Recombinant SARS-CoV Bearing Epidemic and Zoonotic Spike Variants. *PLOS Medicine* **3**, e525 (2006).

45. A. W. Chung, *et al.*, Dissecting Polyclonal Vaccine-Induced Humoral Immunity against HIV Using Systems Serology. *Cell* **163**, 988–998 (2015).

46. M. F. Boni, *et al.*, Evolutionary origins of the SARS-CoV-2 sarbecovirus lineage responsible for the COVID-19 pandemic. *Nat Microbiol* **5**, 1408–1417 (2020).

47. A. T. DiPiazza, *et al.*, COVID-19 vaccine mRNA-1273 elicits a protective immune profile in mice that is not associated with vaccine-enhanced disease upon SARS-CoV-2 challenge. *Immunity* **54**, 1869-1882.e6 (2021).

48. V. D. Menachery, L. E. Gralinski, R. S. Baric, M. T. Ferris, New Metrics for Evaluating Viral Respiratory Pathogenesis. *PLoS One* **10** (2015).

49. E. S. Geanes, *et al.*, Cross-reactive antibodies elicited to conserved epitopes on SARS-CoV-2 spike protein after infection and vaccination. *Sci Rep* **12**, 6496 (2022).

50. C. Wang, *et al.*, A conserved immunogenic and vulnerable site on the coronavirus spike protein delineated by cross-reactive monoclonal antibodies. *Nat Commun* **12**, 1715 (2021).

51. M. Bolles, *et al.*, A Double-Inactivated Severe Acute Respiratory Syndrome Coronavirus Vaccine Provides Incomplete Protection in Mice and Induces Increased Eosinophilic Proinflammatory Pulmonary Response upon Challenge. *J Virol* **85**, 12201–12215 (2011).

52. S. Murakami, *et al.*, Isolation of bat sarbecoviruses of SARS-CoV-2 clade, Japan. *bioRxiv*, 2022.05.16.492045 (2022).

53. A. Schäfer, *et al.*, A Multitrait Locus Regulates Sarbecovirus Pathogenesis. *mBio* **0**, e01454-22 (2022).

54. E. Aleebrahim-Dehkordi, *et al.*, T helper type (Th1/Th2) responses to SARS-CoV-2 and influenza A (H1N1) virus: From cytokines produced to immune responses. *Transpl Immunol* **70**, 101495 (2022).

55. S. Fischinger, *et al.*, A high-throughput, bead-based, antigen-specific assay to assess the ability of antibodies to induce complement activation. *Journal of Immunological Methods* **473**, 112630 (2019).

56. A. Pegu, *et al.*, Durability of mRNA-1273 vaccine–induced antibodies against SARS-CoV-2 variants. *Science* **373**, 1372–1377 (2021).

57. C. S. Tan, *et al.*, Durability of Heterologous and Homologous COVID-19 Vaccine Boosts. *JAMA Network Open* **5**, e2226335 (2022).

58. H. L. Dugan, *et al.*, Profiling B cell immunodominance after SARS-CoV-2 infection reveals antibody evolution to non-neutralizing viral targets. *Immunity* (2021) https:/doi.org/10.1016/j.immuni.2021.05.001 (May 27, 2021).

59. J. Zhao, *et al.*, Airway Memory CD4+ T Cells Mediate Protective Immunity against Emerging Respiratory Coronaviruses. *Immunity* **44**, 1379–1391 (2016).

60. A. J. Greaney, *et al.*, Antibodies elicited by mRNA-1273 vaccination bind more broadly to the receptor binding domain than do those from SARS-CoV-2 infection. *Science Translational Medicine* **13**, eabi9915 (2021).

61. L. Min, Q. Sun, Antibodies and Vaccines Target RBD of SARS-CoV-2. *Frontiers in Molecular Biosciences* **8** (2021).

62. W. N. Voss, *et al.*, Prevalent, protective, and convergent IgG recognition of SARS-CoV-2 non-RBD spike epitopes. *Science* **372**, 1108–1112 (2021).

63. S. Prakash, *et al.*, Genome-Wide B Cell, CD4+, and CD8+ T Cell Epitopes That Are Highly Conserved between Human and Animal Coronaviruses, Identified from SARS-CoV-2 as Targets for Preemptive Pan-Coronavirus Vaccines. *The Journal of Immunology* **206**, 2566–2582 (2021).

64. M. M. Sauer, *et al.*, Structural basis for broad coronavirus neutralization. *Nat Struct Mol Biol* **28**, 478–486 (2021).

65. L. Dai, *et al.*, A Universal Design of Betacoronavirus Vaccines against COVID-19, MERS, and SARS. *Cell* **182**, 722-733.e11 (2020).

66. A. A. Cohen, *et al.*, Mosaic nanoparticles elicit cross-reactive immune responses to zoonotic coronaviruses in mice. *Science* **371**, 735–741 (2021).

67. X.-N. Li, *et al.*, Effectiveness of inactivated SARS-CoV-2 vaccines against the Delta variant infection in Guangzhou: a test-negative case-control real-world study. *Emerg Microbes Infect* **10**, 1751–1759 (2021).

68. K. B. Pouwels, *et al.*, "Impact of Delta on viral burden and vaccine effectiveness against new SARS-CoV-2 infections in the UK" (Epidemiology, 2021) https:/doi.org/10.1101/2021.08.18.21262237 (September 14, 2021).

69. A. Puranik, *et al.*, Comparison of two highly-effective mRNA vaccines for COVID-19 during periods of Alpha and Delta variant prevalence. *medRxiv*, 2021.08.06.21261707 (2021).

70. H. M. Scobie, Monitoring Incidence of COVID-19 Cases, Hospitalizations, and Deaths, by Vaccination Status — 13 U.S. Jurisdictions, April 4–July 17, 2021. *MMWR Morb Mortal Wkly Rep* **70** (2021).

71. R. E. Sealy, J. L. Hurwitz, Cross-Reactive Immune Responses toward the Common Cold Human Coronaviruses and Severe Acute Respiratory Syndrome Coronavirus 2 (SARS-CoV-2): Mini-Review and a Murine Study. *Microorganisms* **9**, 1643 (2021).

72. M. Grobben, *et al.*, Cross-reactive antibodies after SARS-CoV-2 infection and vaccination. *eLife* **10**, e70330.

73. S. Klompus, *et al.*, Cross-reactive antibodies against human coronaviruses and the animal coronavirome suggest diagnostics for future zoonotic spillovers. *Science Immunology* **6**, eabe9950 (2021).

74. C. Dacon, *et al.*, Broadly neutralizing antibodies target the coronavirus fusion peptide. *Science* **0**, eabq3773 (2022).

75. Y. C. Bartsch, *et al.*, Omicron variant Spike-specific antibody binding and Fc activity are preserved in recipients of mRNA or inactivated COVID-19 vaccines. *Sci Transl Med* **14**, eabn9243 (2022).

76. P. Shah, G. A. Canziani, E. P. Carter, I. Chaiken, The Case for S2: The Potential Benefits of the S2 Subunit of the SARS-CoV-2 Spike Protein as an Immunogen in Fighting the COVID-19 Pandemic. *Frontiers in Immunology* **12**, 508 (2021).

77. D. Weiskopf, B. Weinberger, B. Grubeck-Loebenstein, The aging of the immune system. *Transplant International* **22**, 1041–1050 (2009).

78. T. Fülöp, G. Fóris, I. Wórum, A. Leövey, Age-dependent alterations of Fc gamma receptor-mediated effector functions of human polymorphonuclear leucocytes. *Clin Exp Immunol* **61**, 425–432 (1985).

79. S. R. Simmons, M. Bhalla, S. E. Herring, E. Y. I. Tchalla, E. N. Bou Ghanem, Older but Not Wiser: the Age-Driven Changes in Neutrophil Responses during Pulmonary Infections. *Infect Immun* **89**, e00653-20 (2021).

80. N. Rosenthal, S. Brown, The mouse ascending: perspectives for human-disease models. *Nat Cell Biol* **9**, 993–999 (2007).

81. S.-H. Sun, *et al.*, A Mouse Model of SARS-CoV-2 Infection and Pathogenesis. *Cell Host & Microbe* **28**, 124-133.e4 (2020).

82. A. S. Cockrell, *et al.*, A mouse model for MERS coronavirus-induced acute respiratory distress syndrome. *Nature Microbiology* **2**, 1–11 (2016).

1061 83. L. J. White, *et al.*, An alphavirus vector-based tetravalent dengue vaccine induces a rapid
1062 and protective immune response in macaques that differs qualitatively from immunity
1063 induced by live virus infection. *J Virol* **87**, 3409–3424 (2013).

1064 84. N. L. Davis, *et al.*, Alphavirus Replicon Particles as Candidate HIV Vaccines. *IUBMB Life* **53**,
1065 209–211 (2002).

1066 85. M. Wecker, *et al.*, Phase I safety and immunogenicity evaluations of an alphavirus replicon
1067 HIV-1 subtype C gag vaccine in healthy HIV-1-uninfected adults. *Clin Vaccine Immunol* **19**,
1068 1651–1660 (2012).

1069 86. K. Lundstrom, Alphavirus-Based Vaccines. *Viruses* **6**, 2392–2415 (2014).

1070 87. C. M. Boudreau, G. Alter, Extra-Neutralizing FcR-Mediated Antibody Functions for a
1071 Universal Influenza Vaccine. *Frontiers in Immunology* **10** (2019).

1072 88. S. Jegaskanda, The Potential Role of Fc-Receptor Functions in the Development of a
1073 Universal Influenza Vaccine. *Vaccines (Basel)* **6**, 27 (2018).

1074 89. C. M. Boudreau, *et al.*, Dissecting Fc signatures of protection in neonates following
1075 maternal influenza vaccination in a placebo-controlled trial. *Cell Reports* **38**, 110337
1076 (2022).

1077 90. A. G. Dias, *et al.*, Antibody Fc characteristics and effector functions correlate with
1078 protection from symptomatic dengue virus type 3 infection. *Science Translational*
1079 *Medicine* **14**, eabm3151 (2022).

1080 91. Q. He, *et al.*, Immunogenicity and protective efficacy of a recombinant protein subunit
1081 vaccine and an inactivated vaccine against SARS-CoV-2 variants in non-human primates.
1082 *Sig Transduct Target Ther* **7**, 1–11 (2022).

1083 92. S. Bournazos, J. V. Ravetch, Fcγ Receptor Function and the Design of Vaccination
1084 Strategies. *Immunity* **47**, 224–233 (2017).

1085 93. T. T. Wang, *et al.*, Anti-HA Glycoforms Drive B Cell Affinity Selection and Determine
1086 Influenza Vaccine Efficacy. *Cell* **162**, 160–169 (2015).

1087 94. D. J. DiLillo, J. V. Ravetch, Differential Fc-Receptor Engagement Drives an Anti-tumor
1088 Vaccinal Effect. *Cell* **161**, 1035–1045 (2015).

1089 95. L. E. Gralinski, *et al.*, Genome Wide Identification of SARS-CoV Susceptibility Loci Using the
1090 Collaborative Cross. *PLoS Genet* **11**, e1005504 (2015).

1091 96. K. E. Noll, M. T. Ferris, M. T. Heise, The Collaborative Cross: A Systems Genetics Resource
1092 for Studying Host-Pathogen Interactions. *Cell Host & Microbe* **25**, 484–498 (2019).

97. C. E. Edwards, *et al.*, Swine acute diarrhea syndrome coronavirus replication in primary human cells reveals potential susceptibility to infection. *Proc Natl Acad Sci U S A* **117**, 26915–26925 (2020).

98. Y. J. Hou, *et al.*, SARS-CoV-2 Reverse Genetics Reveals a Variable Infection Gradient in the Respiratory Tract. *Cell* **182**, 429-446.e14 (2020).

99. M. Prentiss, A. Chu, K. K. Berggren, Finding the infectious dose for COVID-19 by applying an airborne-transmission model to superspreader events. *PLoS One* **17**, e0265816 (2022).

100. E. P. Brown, *et al.*, Multiplexed Fc array for evaluation of antigen-specific antibody effector profiles. *J Immunol Methods* **443**, 33–44 (2017).

101. G. Lofano, *et al.*, Antigen-specific antibody Fc glycosylation enhances humoral immunity via the recruitment of complement. *Sci Immunol* **3**, eaat7796 (2018).

102. T. M. Narowski, *et al.*, SARS-CoV-2 mRNA vaccine induces robust specific and cross-reactive IgG and unequal neutralizing antibodies in naive and previously infected people. *Cell Rep* **38**, 110336 (2022).

1. Venezuelan Equine Encephalitis Virus Replicon Particle VRP3526 for high-titer vaccinations

A.

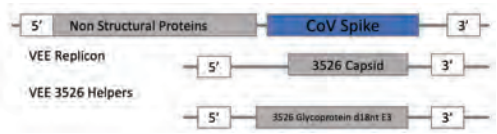

B.

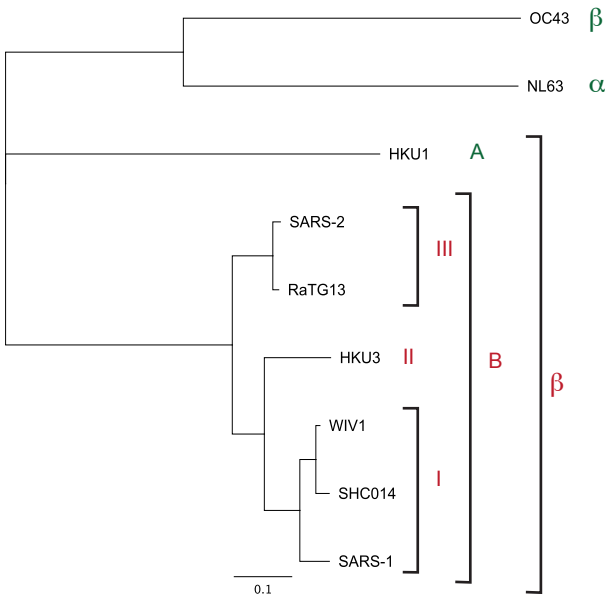

C.

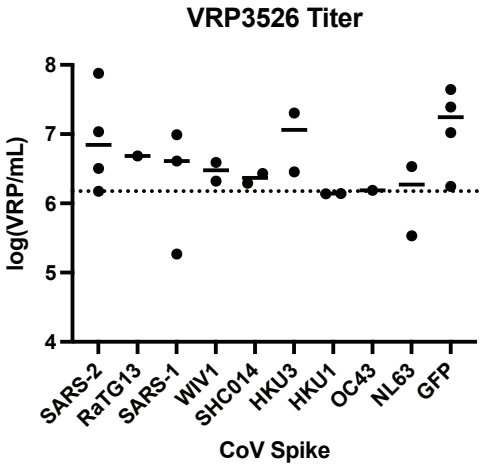

D.

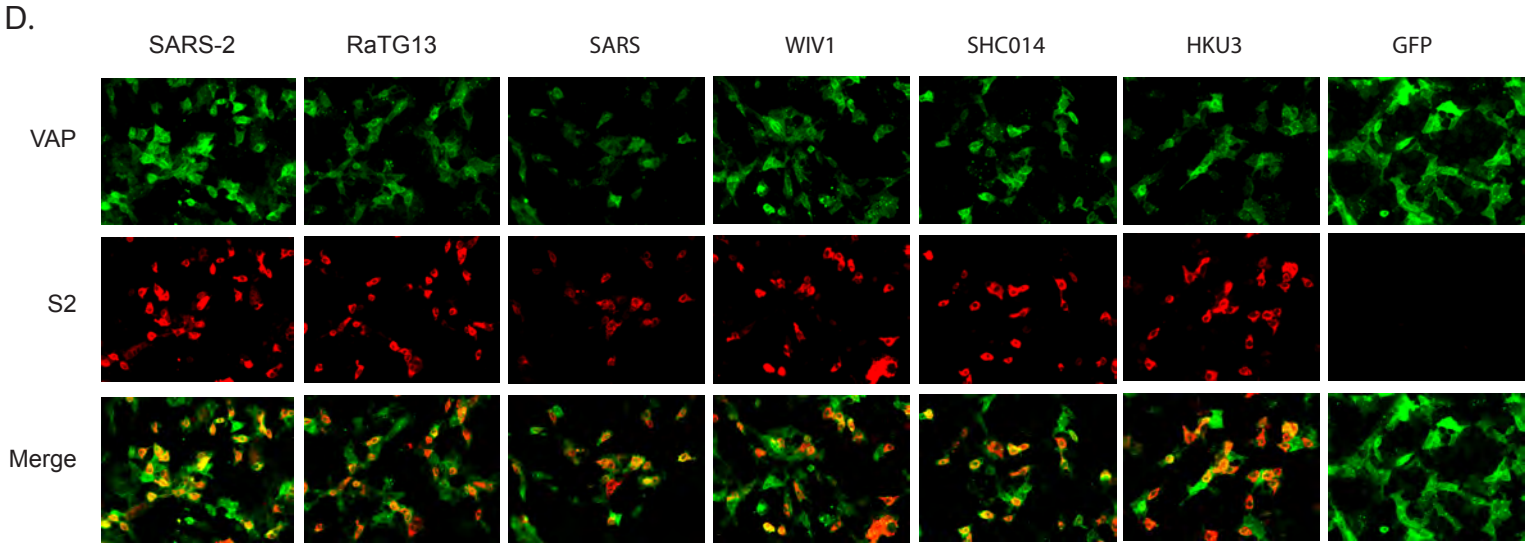

2. VRP Sarbecovirus spike vaccines are cross-protective against SARS-CoV-2 lethal disease

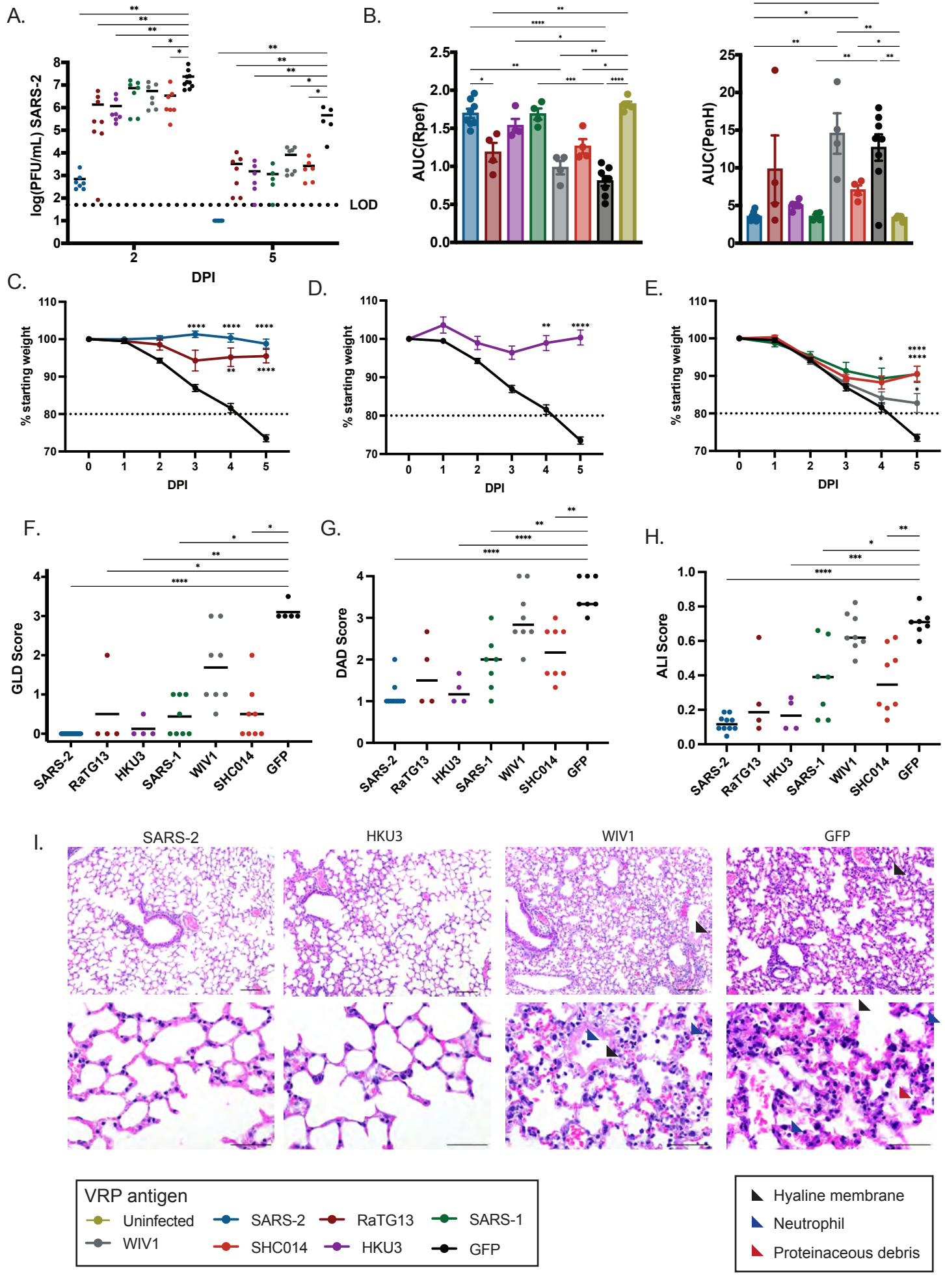

3. VRP Spike protects from lethal infection in vulnerable aged mice

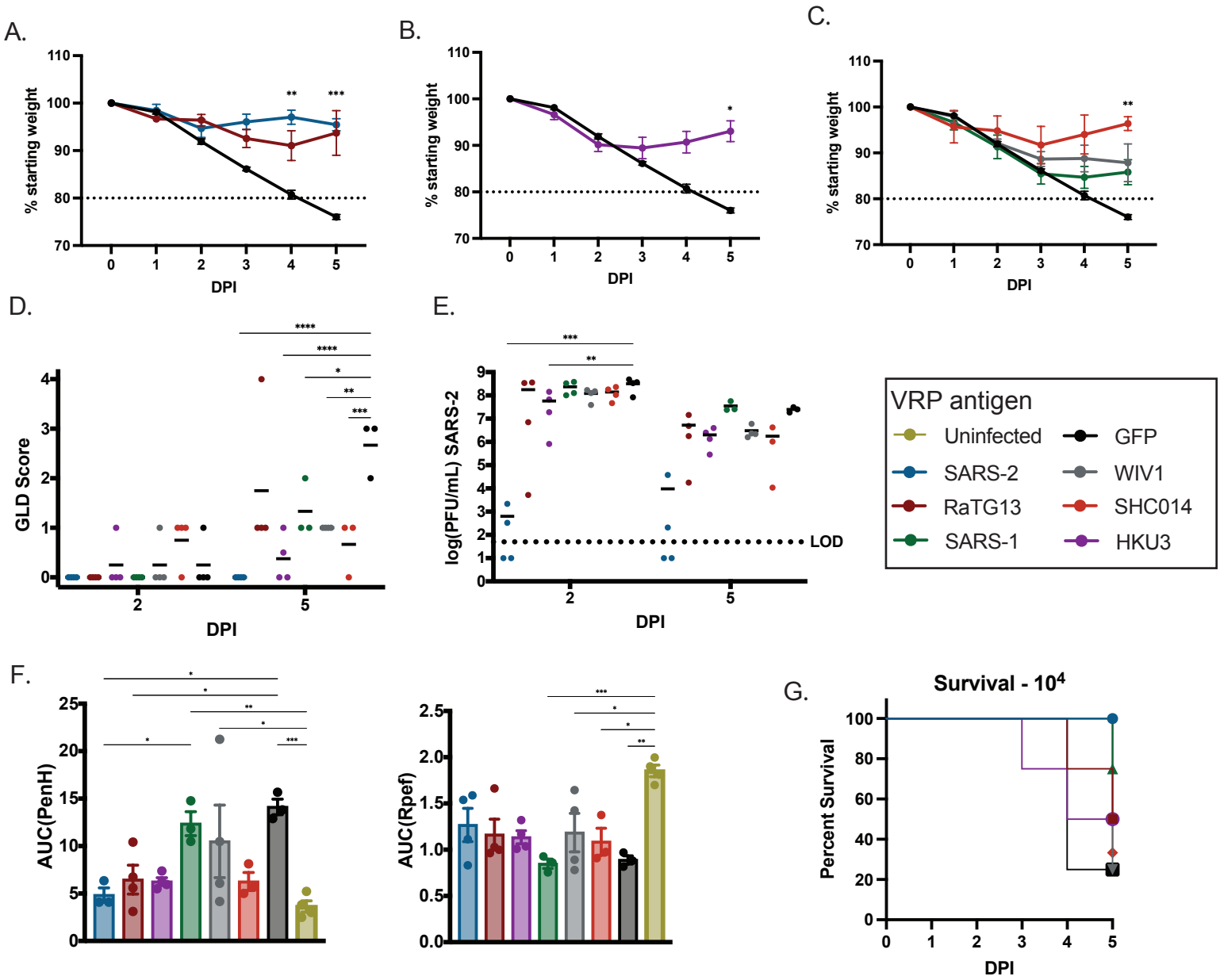

4. VRP SARS-2 spike vaccination protects against heterologous challenge

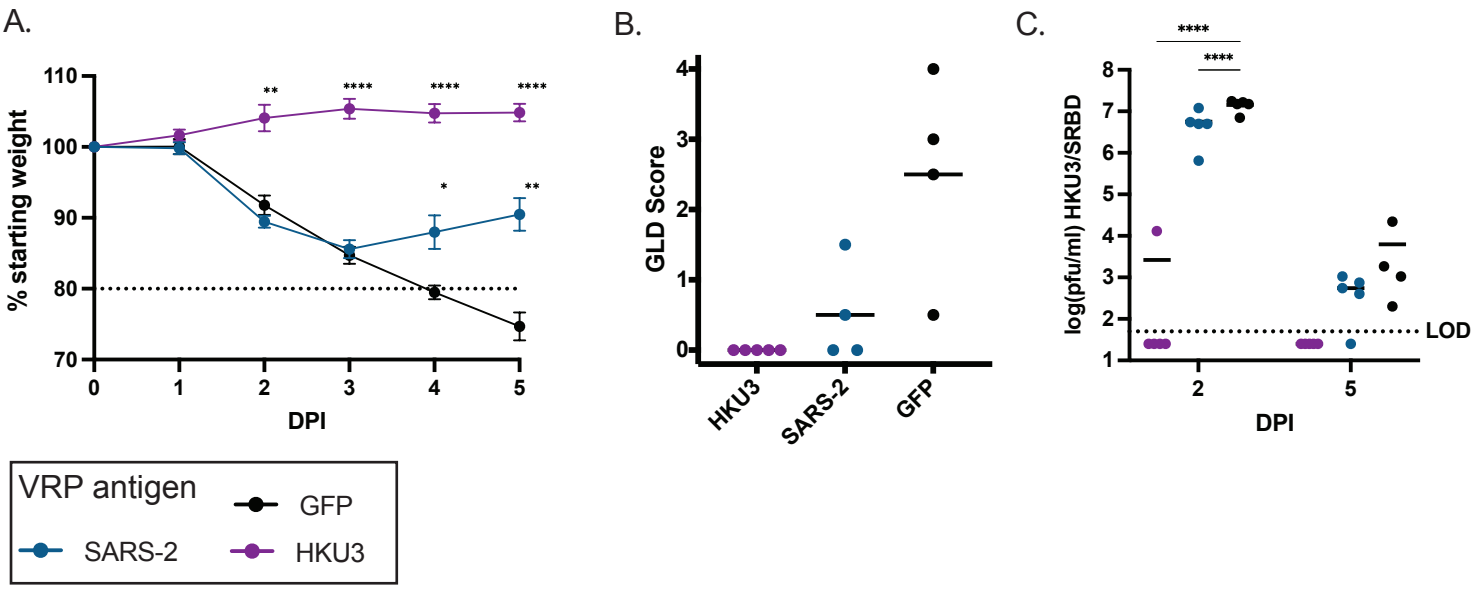

5. Characterizing the antibody response through systems serology and functional assays

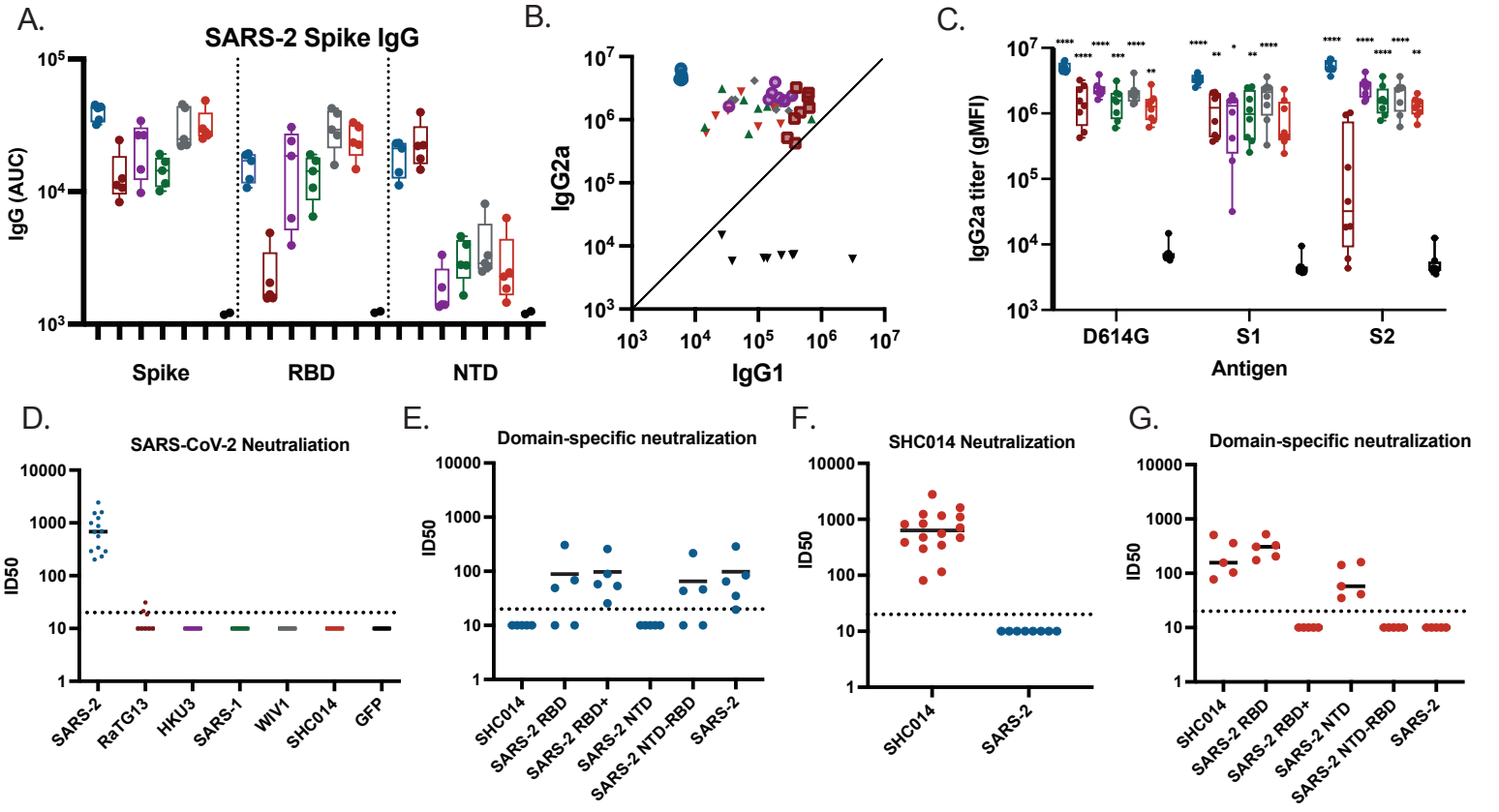

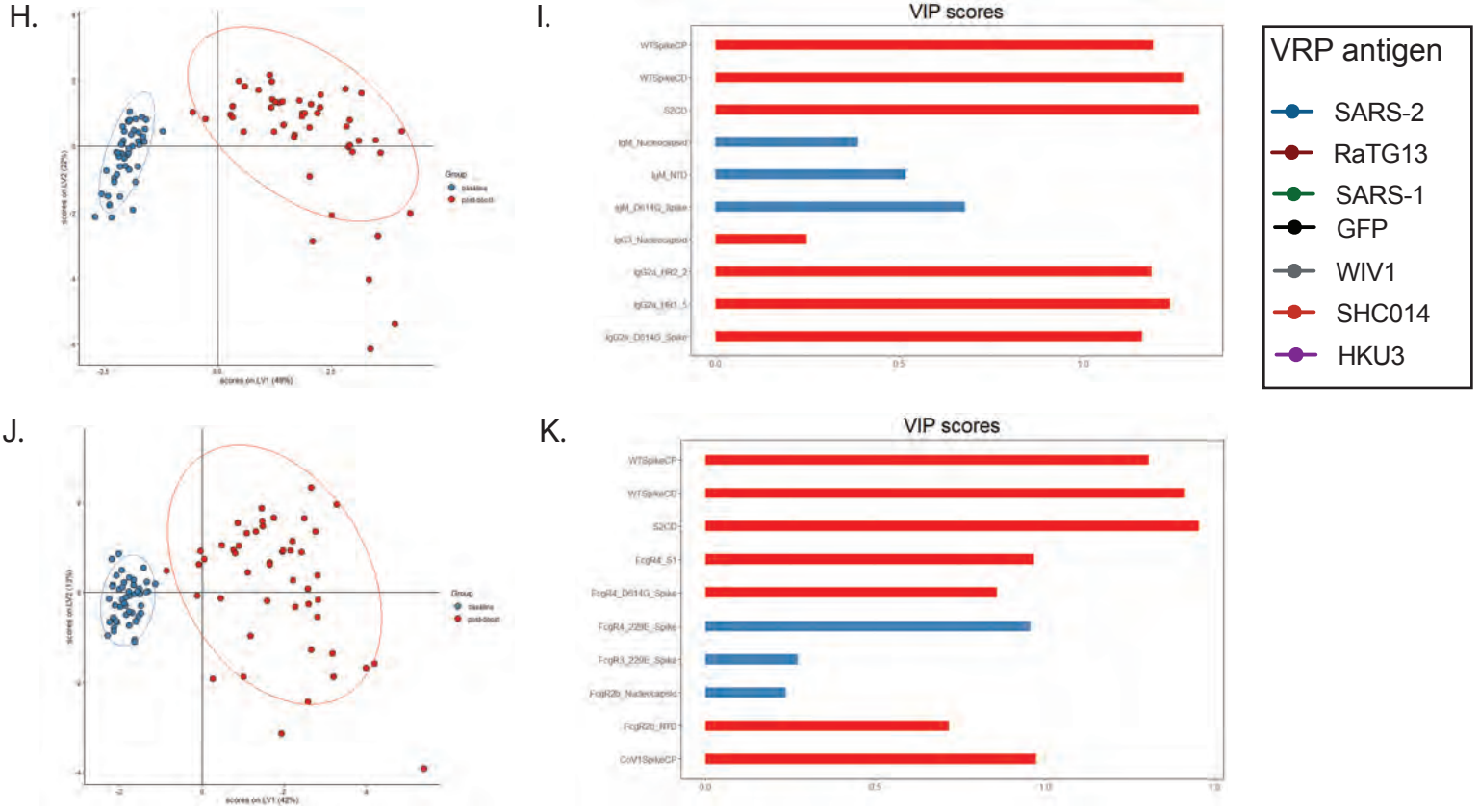

6. Non-neutralizing antibodies mediate protection *in vivo* through Fc function

A.

		IgG2a							
		Spike	S1	S2	NTD	HR1	HR2	FP	Stalk
ADCP	Spike			HKU3 SARS-1 WIV1					
ADNP	Spike			HKU3 SARS-1 WIV1			SHC014 WIV1		SHC014
	S2			HKU3 SARS-1 WIV1			WIV1	HKU3	SHC014
ADCD	Spike			HKU3 SARS-2		SARS-2	RaTG13		
	S2			RaTG13					
FcgR3	Spike	HKU3 RaTG13 WIV1 SARS-2		SARS-2		SARS-2			
	S1	SARS-1	RaTG13						
	S2			HKU3 SARS-2		SARS-2			
FcgR4	Spike	HKU3 RaTG13 WIV1 SARS-2	RaTG13		RaTG13	SARS-2	SHC014	SARS-2	SARS-2
	S1	SHC014 SARS-1 WIV1	HKU3 RaTG13 SHC014 SARS-1		RaTG13	SARS-2		SARS-2	
	S2	SARS-2		HKU3 RaTG13 SHC014 SARS-1 WIV1 SARS-2		SARS-1 SARS-2	SARS-1 WIV1 SARS-2	SARS-1 SARS-2	SARS-1 SARS-2
	NTD				RaTG13	SARS-2		SARS-2